Annual Report

Hydrospheric Atmospheric Research Center (HyARC)

Nagoya University

2006

Annual Report

Hydrospheric Atmospheric Research Center (HyARC)

2006

NAGOYA UNIVERSITY

Contents

Foreword

Six years have passed since the Hydrospheric Atmospheric Research Center (HyARC) at Nagoya University was established to promote research on the global water cycle. The global water cycle is one of the primary components of the Earth system, and its research requires strong and extensive collaboration among the science and application communities. HyARC functions as an inter-university collaborative system, which may be unique in the world. During the last six years, the research style of HyARC has become definite, and specific projects/activities have been initiated and continued. The projects/activities include the operation of the International Project Office of the GEWEX Asian Monsoon Experiment (GAME), a sub-project under GEWEX, led by Prof. T. Yasunari at HyARC, and the promotion of its follow-on projects. There are 3 ongoing major projects supported with the Grants-in-aid for Scientific Research. Two projects are being conducted with the support of the Core Research for Evolutional Science and Technology (CREST) of the Japan Science and Technology Corporation (JST). HyARC has also collaborated with institutions such as the Research Institute of Humanity and Nature (RIHN) and the National Institute of Information and Communication Technology (NICT), and has its own collaborative activities. We have selected a few center research projects to be funded from the HyARC budget. Although funds are limited, the projects are selected based on the feasibility, necessity, and collaboration requirements. We have four center research projects and seven workshops in this fiscal year.

Although the number of permanent staff at HyARC is only 11 (4 professors, 4 associated professors, and 3 assistant professors), many post-doctoral candidates are involved in active research at HyARC. In addition, we have accepted graduate students in the Department of Environmental Studies. As a part of contributing to the UNESCO International Hydrology Programme (IHP), we have conducted an IHP training course, which is funded by the Japan Trust every Japanese fiscal year. This year, the theme of the IHP training course was "Oceanography Basics."

Nagoya University has undergone a major change toward a flexible management system with an emphasis on accountability. At the same time, research publications and other outreach programs are being encouraged.

Uyeda Hiroshi
Director
Hydrospheric Atmospheric Research Center

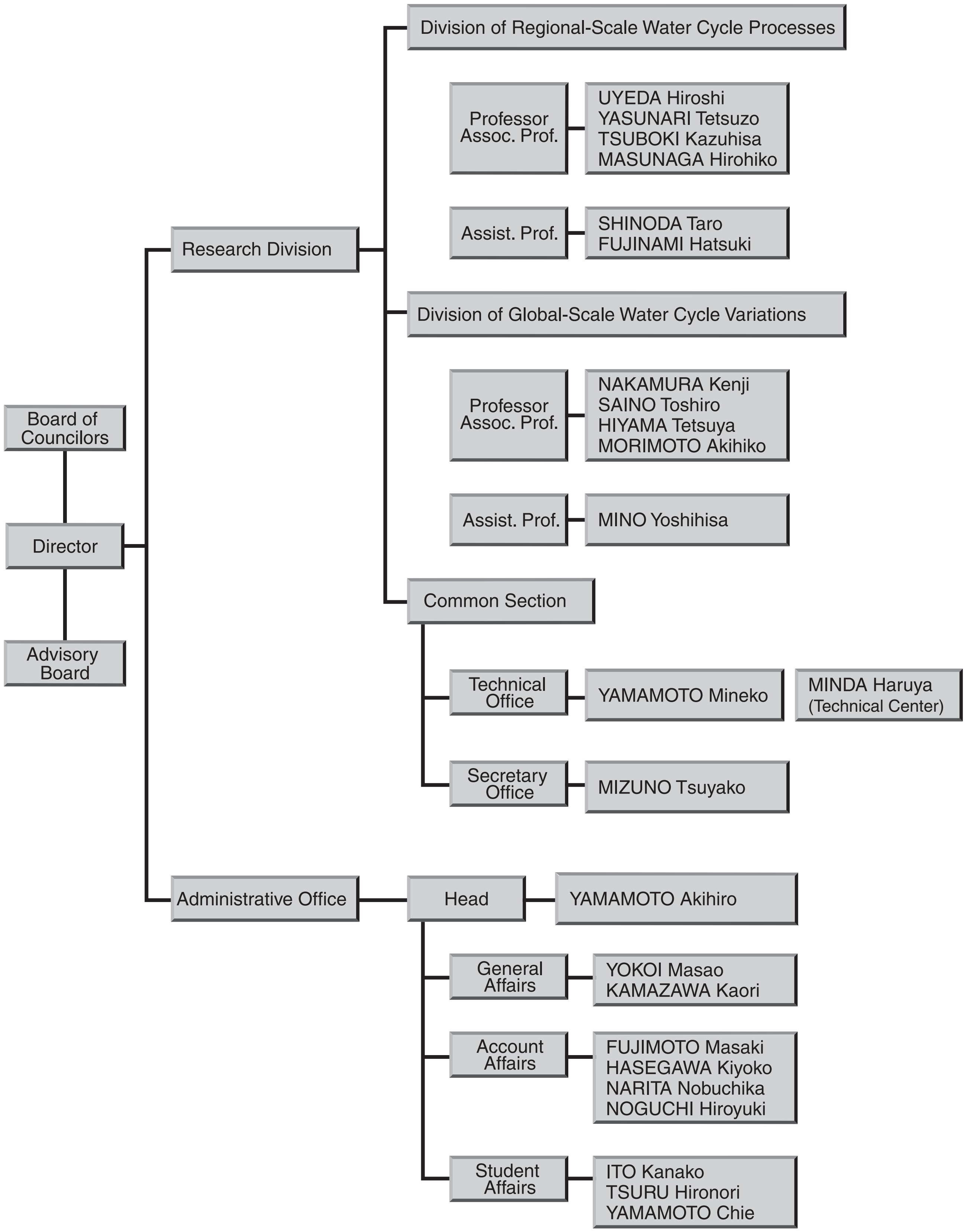
Board of Councilors
Director
Advisory Board
Research Division
Division of Regional-Scale Water Cycle Processes
Professor
Assoc. Prof.
UYEDA Hiroshi
YASUNARI Tetsuzo
TSUBOKI Kazuhisa
MASUNAGA Hirohiko
Assist. Prof.
SHINODA Taro
FUJINAMI Hatsuki
Division of Global-Scale Water Cycle Variations
Professor
Assoc. Prof.
NAKAMURA Kenji
SAINO Toshiro
HIYAMA Tetsuya
MORIMOTO Akihiko
Assist. Prof.
MINO Yoshihisa
Common Section
Technical Office
YAMAMOTO Mineko
MINDA Haruya
(Technical Center)
Secretary Office
MIZUNO Tsuyako
Administrative Office
Head
YAMAMOTO Akihiro
General Affairs
YOKOI Masao
KAMAZAWA Kaori
Account Affairs
FUJIMOTO Masaki
HASEGAWA Kiyoko
NARITA Nobuchika
NOGUCHI Hiroyuki
Student Affairs
ITO Kanako
TSURU Hironori
YAMAMOTO Chie

Administration

Board of Councilors

UYEDA Hiroshi: *Director, Prof., Hydrospheric Atmospheric Research Center*
YASUNARI Tetsuzo: *Prof., Hydrospheric Atmospheric Research Center*
NAKAMURA Kenji: *Prof., Hydrospheric Atmospheric Research Center*
SAINO Toshiro: *Prof., Hydrospheric Atmospheric Research Center*
UEMURA Daisuke: *Prof., Graduate School of Science*
HARAGUCHI Hiroki: *Prof., Graduate School of Engineering*
HATTORI Shigeaki: *Prof., Graduate School of Bioagricultural Sciences*
KANZAWA Hiroshi: *Prof., Graduate School of Enviromentral Studies*
FUJII Ryoichi: *Prof., Solar-Terrestrial Environment Laboratory*

Advisory Board

●Members from Nagoya Unisversity

UYEDA Hiroshi: *Director, Prof., Hydrospheric Atmosphric Research Center*
YASUNARI Tetsuzo: *Prof., Hydrospheric Atmospheric Research Center*
NAKAMURA Kenji: *Prof., Hydrospheric Atmosphric Research Center*
SAINO Toshiro: *Prof., Hydrospheric Atmosphric Research Center*
TSUBOKI Kazuhisa: *Assoc. Prof., Hydrospheric Atmosphric Research Center*
MASUNAGA Hirohiko: *Assoc. Prof., Hydrospheric Atmosphric Research Center*
HIYAMA Tetsuya: *Assoc. Prof., Hydrospheric Atmosphric Research Center*
MORIMOTO Akihiko: *Assoc. Prof., Hydrospheric Atmosphric Research Center*
TSUJIMOTO Tetsuro: *Prof., Graduate School of Engineering*
OHTA Takeshi: *Prof., Graduate School of Bioagricultural Sciences*
AGETA Yutaka: *Prof., Graduate School of Environment Studies*
MATSUMI Yutaka: *Prof., Solar-Terrestrial Environment Laboratory*

●Members outside Nagoya University

FUJIYOSHI Yasushi: *Prof., Institute of Low Temparature Science, Hokkaido University*
HANAWA Kimio: *Prof., Graduate School of Science, Tohoku University*
SUMI Akimasa: *Prof., Center for Climate System Research, The University of Tokyo*
FUKUSHIMA Yoshihiro: *Prof., Research Intutite for Humanity and Nature*
YAMANAKA Manabu: *Senior Scientist, Institute of Observational Research for Global Change, Japan Agency for Marine-Earth Science and Technology*

Diurnal processes of convection/precipitation systems in the climate system

Diurnal variation in convection and precipitation is a prominent meteorological feature, particularly in the tropics/subtropics and monsoon regions. Energy, water and momentum exchanges through the diurnal cycle between the earth surface, atmospheric boundary layer and free atmosphere play a crucial role in the global climate system. Recently, high-resolution satellite (e.g., MTSAT, TRMM) data in time-space become available to use for studies on the diurnal cycle. However, climate models (i.e. GCM) can still not reproduce a realistic diurnal cycle in convection/precipitation, inducing systematic errors in the models.

This research plan aims to clarify regionality and seasonality of diurnal processes based on TRMM, other remote sensing data and *in-situ* observational data from raingauge stations. Cloud resolving models (e.g. CReSS andWRF) and other regional models are also used to elucidate systematic errors on the climate model due to the diurnal cycle. These researches can contribute to ongoing international project “MAHASRI”. We aim to promote studies in diurnal processes of convection/precipitation in the climate system in Japan.

On 14th July 2006, a domestic workshop, co-hosted by MAHASRI, was held on this topic at Yokomaha Institute for Earth Sciences/ JAMSTEC. 13 presenters and many participants attended the workshop, and valuable discussions were held on the issues described above. On 9th March, a second domestic workshop related to this research plan was held in Hakone. Studies on diurnal cycle of cloud/precipitation systems, including a relationship with land terrain, an interaction between the diurnal cycle and intraseasonal variation, long-term trend, etc, were presented. 13 presenters made presentations in the new scientific results and made a lively discussion with many participants in the workshop.

High-Resolution Modeling of Atmospheric Water Circulation Systems Using Cloud-Resolving Model

Clouds and precipitation systems have multi-scale structures ranging from a single-cell cloud to a large-scale weather system. Each class of the multi-scale structures has its own properties and roles in precipitation systems. For simulations of the multi-scale structure of precipitation systems, extensive computation using a cloud-resolving model is necessary. The purpose of this research is explicit simulations of clouds and organized precipitation systems using the cloud-resolving model in a large domain and a very fine grid (less than 1 km). In this research, we utilized the Cloud Resolving Storm Simulator (CReSS), which is a cloud-resolving model developed for parallel computers. Using CReSS on the Earth Simulator, we performed simulation experiments of important cloud and precipitation systems.

One of the important objectives of high-resolution simulation is a typhoon. We briefly summarize the result of the simulation experiment for Typhoon 0613 (T0613), which was accompanied by intense tornadoes ("tatsumakis" in Japanese) along the east coast of Kyushu. The horizontal grid spacing of the simulation experiment of T0613 was 500 m. The CReSS model simulated the overall structure and movement of T0613 and detailed structures of associated rainbands. Figure 1 shows a close-up view of the simulated rainband, which formed to the east of Kyushu. The rainband is composed of convective clouds. Some of these are super-cells, as indicated by the rectangle in the figure. The east-west vertical cross section shows that one of the super-cells has a vault structure and intense vorticity in the cell (Fig. 2).

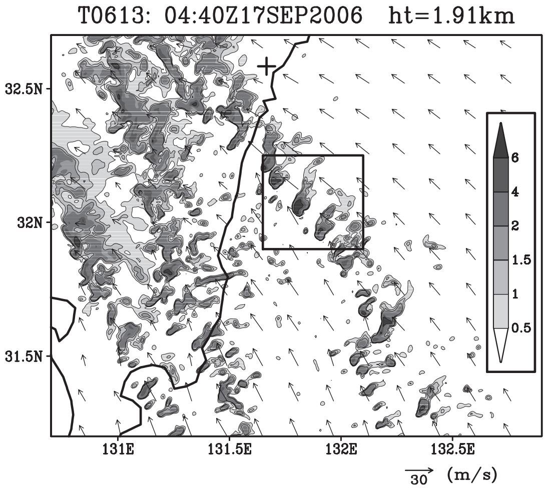

Figure 1 Close-up view of typhoon rainbands obtained from a 500 m-resolution experiment using the CReSS model at 0440 UTC, September 17, 2006. Gray scales indicate the rain mixing ratio (g kg^{-1}) at a height of 1.91 km. Arrows are surface wind vectors. The rectangle indicates a region where super-cells are formed.

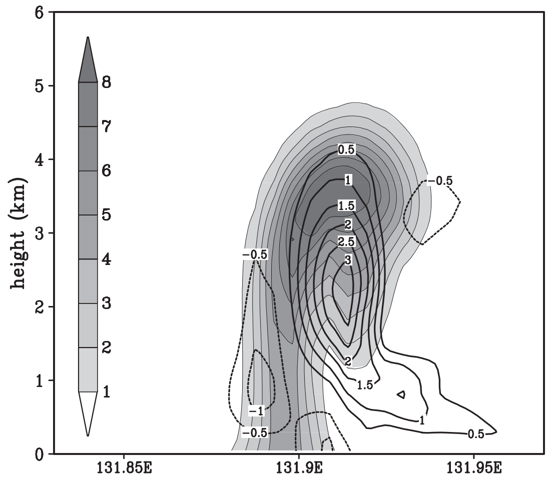

Figure 2 Vertical cross section along the zonal direction at latitude of 31.95 N obtained from the 500 m-resolution experiment at 0440 UTC, September 17, 2006. Gray scales are the mixing ratio of precipitation (g kg^{-1}) and contours are vorticity (10^{-2} s^{-1}).

A higher-resolution simulation with a horizontal grid size of 75 m was also performed to simulate the tatsumaki. The detailed structure of the super-cell was simulated (Fig. 3). A significant hook-shaped structure is formed in the southernmost part of the cell. The intense tatsumaki is formed in the hook-shaped structure, which is indicated by the circle in the figure. The maximum vorticity is 0.9 s^{-1} and pressure perturbation is 24 hPa. The vertical cross section (Fig. 4) shows that the tatsumaki extends up to a height of 2.5 km with a leaning to the north. The cloud is lower in the central part of the tatsumaki. This is similar to a funnel cloud.

The simulation experiments using the CReSS model range from the typhoon scale to the tatsumaki scale, and resolve every class of the multi-scale structure. Such super-high resolution calculations provide detailed data concerning weather systems. Using the output data of these experiments, modeling studies will clarify not only the structure of weather systems but also the interaction between different classes of scale. High-resolution simulations will contribute an accurate and quantitative prediction as well as prevention/reduction of disasters caused by high-impact weather systems.

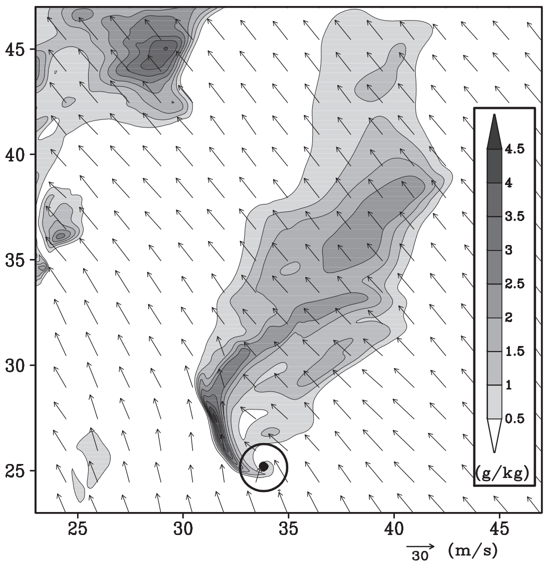

Figure 3 Super-cell with tatsumaki simulated in the 75 m-resolution experiment using the CReSS model at 0500 UTC, September 17, 2006. Gray scales are the rain mixing ratio (g kg^{-1}), and arrows are horizontal wind vectors at a height of 200 m. The circle indicates the tatsumaki forms in the southernmost part of the super-cell.

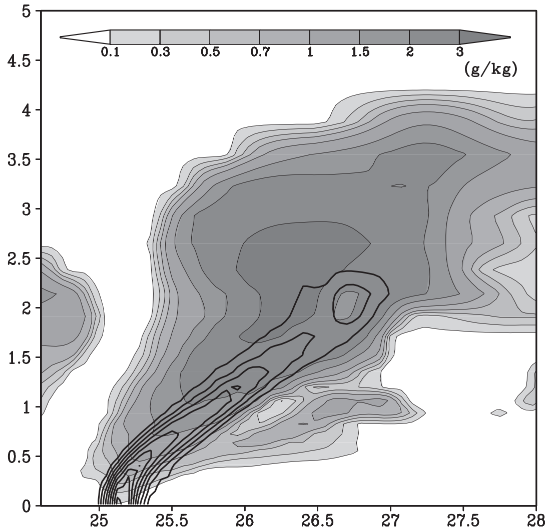

Figure 4 Vertical cross section along the north-south axis of the tatsumaki indicated by the circle in Fig. 3. Gray scales are the cloud mixing ratio (g kg^{-1}) and contours are vorticity.

Application of stable isotopes of water for evaluation of multi-scale water cycle processes

Stable isotope ratios of water (δD & $\delta^{18}O$) and those anomalies from well-known meteoric water line (d-excess = $\delta D - 8 \cdot \delta^{18}O$) are good indicators to identify origins of precipitation, river water, groundwater etc. Since isotope ratios of water are controlled by kinetic or equilibrium fractionation processes in evaporation or condensation, the ratios are applicable for evaluations of global water cycles as supporting tools for water balance calculation, paleoclimate variations, and basin-scale hydrological studies.

HyARC is conducting mass spectral analyses of stable isotope ratios of water as one of the HyARC Research Programs. In fiscal 2006, we comprehensively analyzed 2400 water samples upon request from 11 domestic researchers.

We applied for a research grant to the Japan Society for the Promotion of Science (JSPS) and were accepted for our research plan "Comprehensive Study on Meso-Scale Precipitation System with Use of Stable Isotope Ratios of Water" from fiscal 2005 through 2007. We are also proposing several other methodologies to evaluate multi-scale water cycles in the hydrological processes of evapotranspiration, atmospheric boundary layer process, cloud development, and precipitation processes. Our current targets are:

1) Use of stable isotope ratios of water to understand the mechanism of meso-scale water cycle systems in coordination with other precise meteorological measurements (e.g., multi-band radars, radio soundings, and raindrop size measurements) together with objective reanalyzed data sets, and
2) Use of stable isotope ratios of water to model multi-scale water cycle processes.

This research plan also aims to promote studies in isotope hydrology and to link activities from the multi-scale point of view in water cycles among several research groups in Japan. We are conducting annual science workshops related to this research plan. In fiscal 2006, we held a workshop from 27 to 28, February 2007. Thirty-two participants attended the workshop, and valuable discussions were held on the issues described above.

Observational study on atmosphere and ocean over and around Okinawa Island

The National Institute of Information and Communication Technology (NICT) established an observation center in Okinawa. The facilities of the center include a full polarimetric Doppler radar (COBRA), a 400-MHz wind profiler radar, a Doppler sodar, disdrometers, rain gauges, and ocean radars. The collaboration between NICT Okinawa and HyARC began in 2005. Utilization of the facility was encouraged as one of the inter-university collaboration activities of HyARC.

Analyses of the polarization radar data, wind profiler data, and ocean radar data were continued. The height characteristics of the bright band in the convective precipitation system were investigated from COBRA data. Diurnal variation of the low-level jet in the Baiu season was revealed from the wind profiler radar data. A good comparison of the Kuroshio current between the ocean radar data and the satellite data was obtained. Test-level experiments including ocean observation using COBRA were also conducted. These results were presented at a workshop at NICT Headquarters, Tokyo, in March 2007.

Progress of the 21st Century COE Program "Dynamics of the Sun–Earth–Life Interactive System (SELIS)"

Only one year is remaining before the 21st Century COE Program for the "Sun–Earth–Life Interactive System" (SELIS-COE) ends. During this program, we have promoted interdisciplinary studies on the SELIS, such as the solar activity and glacier mass balance and the role of vegetation in the climate system. Further studies are being conducted as part of various science workshops. Since the 2004 school year, we have opened a special class on "Chikyu-gaku" (Study on the Earth) as part of graduate studies at the graduate school of the environmental sciences. In this class, various COE-related professors give lectures on the earth system and its variations. Besides the class, we are currently preparing a comprehensive textbook on "Chikyu-gaku," which will be issued in fall 2007.

The SELIS-COE program organized an international symposium on "Dynamics of the Ice Age Climate" in Nagoya on November 13–15, 2006. The aim of this program was to integrate the updated information and knowledge on the Ice Age climate reconstruction and modeling, and to comprehensively discuss some unresolved key issues on the Ice Age climate in the past several million years. This will also have deep implications for the current global-warming climate issue. The following keynote speakers were invited from abroad: Jean Jouzel (ice core studies for Antarctica), An Zhishang (sediment studies for the Chinese Loess Plateau), Alexander Prokopenko (sediment core studies for Lake Baikal), Shukuro Manabe (General Circulation Model (GCM) studies), Bette L. Otto-Bliesner (GCM studies), Andrey Ganopolski (Earth System Model for Intermediate Complexity (EMIC) studies), and Michel Crucifix (EMIC & GCM studies). The following topics were discussed in the symposium:

1) What caused the transition of global glaciation features (i.e., periodicity, skewness, and responses to insolation) from the Pliocene to the Pleistocene (5–3 Ma)? 2) What caused the transition in the glacial cycles (from 40- to 100-kyr cycles) around 1 Ma? 3) Modulation of glacial cycles during 1 Ma. 4) What triggers the interglacial to glacial phase in the 100-kyr cycle? 5) Millennial-scale events in the last glacial period.

More than 100 scientists participated in this symposium, and they had heated discussions for the entire three day period.

Core Research for Evolutional Science and Technology (CREST)

● Lower Atmosphere and Precipitation Study (LAPS)

The Lower Atmosphere and Precipitation Study (LAPS) is one of the projects of the Core Research for Evolutional Science and Technology (CREST) of the Japan Science and Technology Agency (JST). The CREST projects are conducted with strategic research themes (http://www.jst.go.jp/kisoken/en). LAPS comes under the theme of "R&D in Hydrological Modeling and Water Resources Systems" supervised by Prof. K. Musiake, Fukushima University. The objective of LAPS is to clarify the relationship between the planetary boundary layer (PBL) and the precipitation system. This year was the final year of this project, and the results were presented at the CREST water theme symposium and our internal workshop.

Important results are the seasonal change in the atmospheric boundary layer (ABL) and the large eddy simulation (LES). The observation showed the changes in the sensible and latent heat fluxes from the surface and the development of the ABL according to the changes in the surface conditions. The observation, however, does not show the profiles of the fluxes in the ABL. The simulations were based on the observation, and after confirming that the simulation reproduced the observation results well, the internal structures of both the ABL and the fluxes were obtained. The results may be summarized as follows. Over dry land, the profile of the fluxes is like a textbook one, i.e., a sensible heat flux with its maximum at the surface is the primary driving force of the ABL. The entrainment layer is also well reproduced. Over wet land, the development of the ABL is weak and water vapor contribution to the buoyancy flux is important. Over sub-tropical ocean, the flux is small and water vapor contribution to the buoyancy flux is of primary importance. Over undulating terrain, the orographic uplift is also important.

Solution Oriented Research in Science and Technology (SORST)

● Satellite Monitoring of Ocean Primary Productivity

Oceans comprise the largest reservoir of water and carbon dioxide on the Earth's surface; hence, the air-sea exchange of water and carbon dioxide plays a central role in determining the planet's climate system. Air-sea exchanges of heat (water) and carbon dioxide are affected by phytoplankton, since these organisms determine the optical properties of near-surface oceans and absorb carbon dioxide through primary productivity. Quantitative knowledge of the abundance and productivity of phytoplankton on a global scale is required for a mechanistic understanding of their regulating processes to improve climate prediction models and thus better predict climate variability. Practically speaking, this knowledge and understanding is attained only by means of satellite observations, but because of difficulties in obtaining in situ data for validation, the satellite data are yet to be fully exploited.

To overcome these difficulties, we have been developing an in situ ocean primary productivity monitoring system to validate primary productivity data obtained from satellites. Comprising an underwater winch system with a profiler buoy equipped with a fast repetition rate fluorometer, the system was successfully developed with the support of the Japan Science and Technology Agency's Core Research for Evolutional Science and Technology program. Following the system's development, a continuation project, "Satellite Monitoring of Ocean Primary Productivity (SMOPP)," was approved by JST in the Solution Oriented Research for Science and Technology Program in 2004. The goal of the SMOPP project is to design an operational system to monitor ocean primary productivity on a global scale. To achieve this goal, we plan to conduct routine operation of the monitoring system and obtain validated time-series satellite data of primary productivity, which is to be utilized in combination with other time-series satellite data on physical forcing parameters on the ocean surface for process studies of the response of ocean biology to the atmospheric forcing on the ocean.

Research activities in FY 2006 on the SMOPP project are described separately in the activity report of the Ocean Climate Biology Lab, with notable achievements including successful operation in the deep western subarctic Pacific for 1.5 months and completion of two full sets of underwater winch systems for continuous time-series operation. As for the Primary Productivity Pofiler, we continued efforts to conduct measurements to the greatest possible extent in various environments, such as the northern North Pacific, Bering Sea, East China Sea, Sea of Japan, and Upper Gulf of Thailand, in addition to Sagami Bay, where test mooring of the buoy system is being carried out.

The process study using multi-parameter satellite data will be carried out for Sagami Bay. To validate the satellite-based process study, cruises of JAMSTEC's Tansei Maru as well as development of the physical-biogeochemical model were conducted for observational studies of rate processes relating to oxygen metabolism in the bay.

Laboratory of Meteorology

Characteristics of mesoscale convective systems over the east part of continental China during the Meiyu period from 2001 to 2003

Hefei Doppler radar observation data over the downstream region of the Yangtze River during the Meiyu period from 2001 to 2003 were analyzed to reveal the predominant structural characteristics of meso-β-scale convective systems (MβCSs) around the Meiyu front. Convective and stratiform portions were separated from MβCSs using the bright band fraction (BBF) method. The daily and yearly mean vertical profiles of radar reflectivity for the convective portion were calculated.

Results showed that the vertical profile of the convective portion of MβCSs for 3 years was characterized by low-altitude radar reflectivity peaks (around 3 km) and large decrease of reflectivity with height above the melting level (Fig. 1). To understand these characteristics of MβCSs, the convection of medium depth (CMD) is defined as a group of convective cells whose echo-top height with a reflectivity of 15 dBZ is equal to or less than 8 km, and the reflectivity peak is below 4 km throughout their lifetime.

To investigate the structural characteristics of MβCSs around the Meiyu front, observed MβCSs were categorized into slow-moving ($\leqq$3 m s^{-1}) and south-of-front (SSF) type, slow-moving and along-the-front (SAF) type, fast-moving ($\geqq$7 m s^{-1}) and along-the-front (FAF) type, and slow-moving and north-of-front (SNF) type according to their movement speed and their locations relative to the surface front (Fig. 2). The predominant convection in the SSF type was the CMD, which covered 51% of the convective area. The CMD and deep convections (DC) coexisted in the SAF, with the CMD covering 34% of the convective area. The FAF type was organized from the DC, and the SNF type primarily consisted of the CMD. The environmental conditions under which the SSF type formed were characterized by a weak wind convergence ($<2 \times 10^{-5}$ s^{-1}) near the surface, a low level of neutral buoyancy, and humid atmosphere below the middle level. The large contribution of the CMD to the convective rainfall amount in the SSF type and its non-negligible contribution to the SAF type indicate that the CMD is one of the main structures of the Meiyu frontal convective precipitation system.

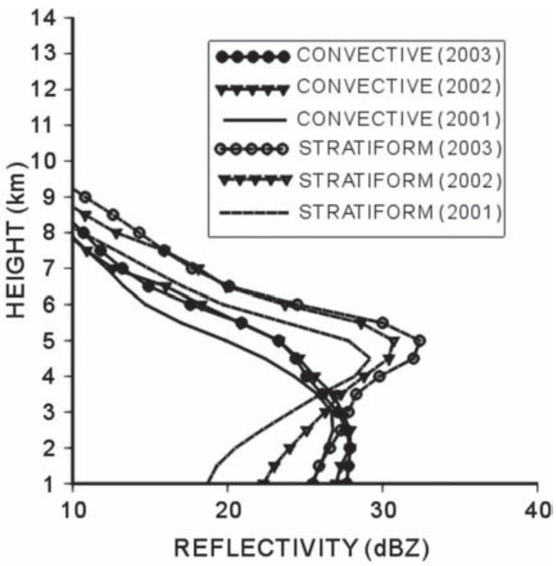

Fig. 1 Yearly mean vertical profile of reflectivity for convective and stratiform portions identified by the BBF method in 2001, 2002, and 2003 within a radar radius of 60 km.

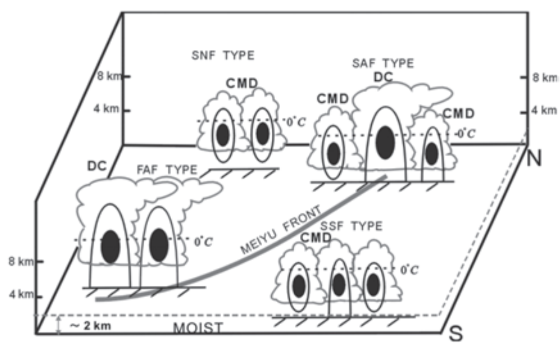

Fig. 2 Schematic illustration of convections for four types of meso-β-scale convective systems around the Meiyu front. The thick solid line indicates the surface front. The dashed line passing through the cloud represents the melting level. CMD and DC represent convection of medium depth and deep convection, respectively. The black ellipse represents the convection core. The line surrounding the black ellipse represents the precipitation region.

Statistical features of precipitation cells observed in East Asia during the Meiyu/Baiu period

To clarify the statistical features of precipitation cells during the Meiyu/Baiu period, Doppler radar data obtained at Shouxian, Anhui Province, China (continental area) from June 17 to July 17, 1998, at Zhouzhuang, Jiangsu Province, China (coastal area) from June 10 to July 13, 2001, and at Okinawa (oceanic area) from May 27 to June 11, 2004 are analyzed. From the radiosonde observations, moist layers were found to exist in the lower (less than 2 km) and middle troposphere (from 2 to 5 km). The following features of precipitation cells over the moist environment in East Asia are obtained: area (horizontal scale), echo-top height, height of maximum reflectivity in each precipitation cell, and vertical gradient of maximum reflectivity above the melting level. In particular, echo-top height and vertical gradient of maximum reflectivity above the melting level are described in detail.

The numbers of analyzed precipitation cells are 2978 at Shouxian, 17529 at Zhouzhuang, and 5093 at Okinawa. The averaged areas of precipitation cells are 16.8 km^2 at Shouxian, 22.8 km^2 at Zhouzhuang, and 16.4 km^2 at Okinawa. There is a tendency for the higher precipitation cells to have a larger area, although this is not clear for cells over 20 km^2.

Figure 3 shows the integrated probability density of echo-top height. The ratio of echo-top height that does not exceed the height of the melting level + 1 km is 69.0% at Shouxian, 74.1% at Zhouzhuang, and 80.8% at Okinawa. Precipitation by warm rain should be effective in these areas.

Figure 4 shows vertical profiles of maximum reflectivity at each level. The fact that the vertical gradient of reflectivity above the melting level over the oceanic area is larger than that over the continental area is well known. However, in this study, the vertical gradient of reflectivity above the melting level at Zhouzhuang (coastal area) and Shouxian (continental area) is not obviously small compared with Okinawa (oceanic area). These observations can be attributed to the moist condition in the lower and middle troposphere. In this condition, it would be difficult to develop deep convection because convective instability is easily consumed by convection and is not accumulated. Therefore, almost all of the precipitation cells in the moist environment frequently observed in East Asia during the Meiyu/Baiu period have echo-top heights that reach only to the melting level + 1 km and large vertical gradient of reflectivity above the melting level.

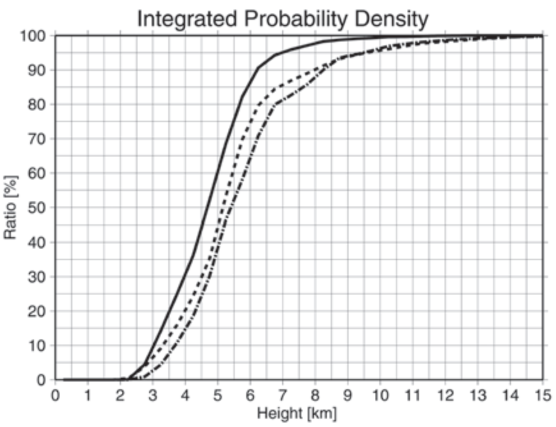

Fig. 3 Integrated probability density of echo-top height at each area. Solid, broken, and dashed lines show Okinawa, Zhouzhuang, and Shouxian, respectively.

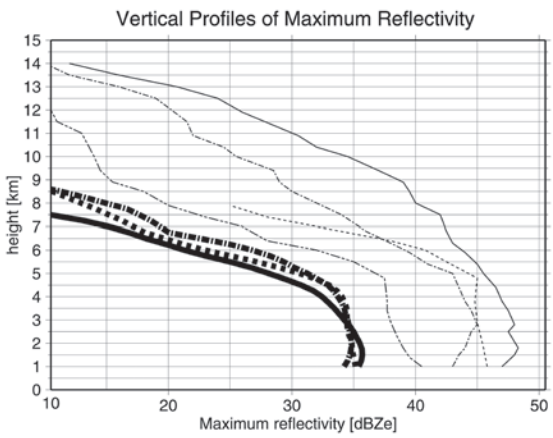

Fig. 4 Vertical profiles of maximum reflectivity. Thick solid, thick broken, and thick dashed lines show Okinawa, Zhouzhuang, and Shouxian, respectively. Thin solid, thin broken, thin dashed, and thin double-dashed lines show Oklahoma (continental), Taiwan (oceanic), Darwin (continental), and Darwin (oceanic) from Zipser and Lutz (1994), respectively.

Detailed structure of velocity and moisture fields around the Baiu frontal zone

Previous studies have revealed that the Baiu frontal zone has complicated rainfall distributions. Moteki et al. (2004) revealed the detailed wind and moisture fields that determine one of the typical Baiu frontal rainfall distributions. There were three airstreams: cold and dry northeasterly, oceanic southwesterly, and comparatively moist continental airstream from the west. On June 27, 2004, we conducted aircraft observation of the Baiu frontal zone around the East China Sea to reveal these structures and found a new cloud pattern unaccountable by the structure shown in Moteki et al. (2004). This implies another structure in the Baiu frontal zone.

Therefore, we conducted another aircraft observation on June 23, 2005. First, we observed the meridional profile at 500 m from 31°N to 25.5°N along 125.9°E. Second, we conducted dropsonde soundings from 12000 m at 4 points (25.9°N, 27.0°N, 28.0°N, and 29.5°N).

Figure 5 shows the results of the 500 m flight. There are two ascending areas: X was weak and wide (28–29.8°N); Y was strong and narrow (26.2–26.8°N). Corresponding to these ascending areas, there were two wind shears: northeast-southwest for X and west-southwest for Y, respectively. Ascending area X had weak precipitation, while ascending area Y had heavy rainfall. Moisture contrast was apparent around the northern edge of the ascending area X. Figure 6 shows the results of dropsonde soundings. Dropsonde points were located at the north and south sides of each ascending area. To the south of the ascending area Y (dropsonde 1), the lower level below 500 m was very moist and convective unstable. To the north of the ascending area Y (dropsonde 2) and south of the ascending area X (dropsonde 3), the atmosphere was comparatively moist and weakly convective unstable. To the north of the ascending area X (dropsonde 4), there was convective neutral stratification and low-level cold inflow.

To understand the detailed structure of the Baiu frontal zone, we performed numerical simulations using the Cloud Resolving Storm Simulator (CReSS). Back-trajectory analysis revealed the wind field around the Baiu frontal zone. As shown in Fig. 7, there were four airstreams: northeasterly, west-southwesterly, southwesterly-1, and southwesterly-2. The atmospheric properties of these airstreams correspond to the features shown in dropsonde 4, 3, 2, and 1, respectively. The convergence among these four airstreams, which had different moisture stratifications, resulted in northern weak and southern heavy rainfall.

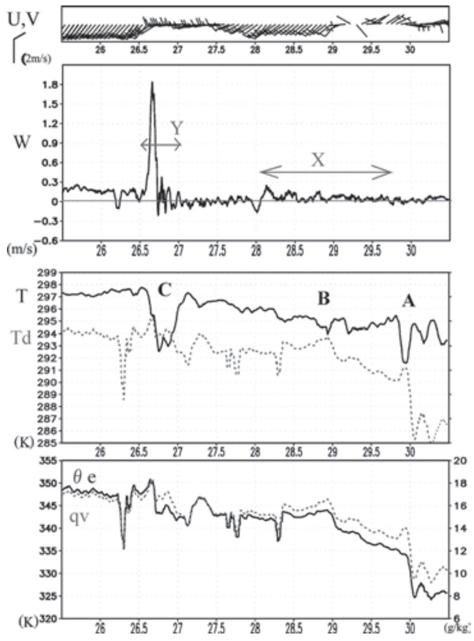

Fig. 5 Meridional profiles of horizontal wind, vertical wind, temperature and dewpoint temperature, and equivalent potential temperature and mixing ratio of water vapor on June 26, 2005.

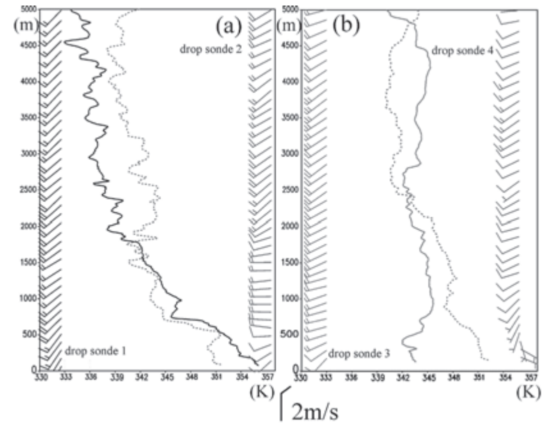

Fig. 6 Vertical profiles of equivalent potential temperature obtained from the dropsonde soundings.

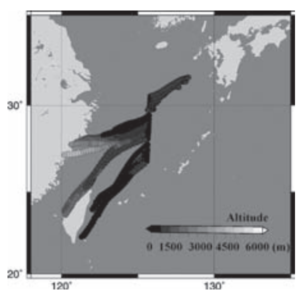

Fig. 7 Back-trajectory analysis chasing 30 airmasses at 500 m height along 125.5° E. Gray scale shows altitude.

Structure of cloud cluster observed by Doppler radar in the tropical western Pacific region on July 1–2, 2005

The aim of this study is to examine the structure of cloud clusters that develop into tropical cyclones in the tropical western Pacific region. We carried out observations on cloud clusters with two Doppler radars in the Republic of Palau in the tropical western Pacific region from June to July 2005. A cloud cluster of 1000-km diameter passed the Republic of Palau from July 1 to 2 (Fig. 8) and developed into a tropical cyclone over the Philippines from July 3 to 4. In this study, the structure of the cloud cluster was examined in detail with Doppler radar data before its development into a tropical cyclone.

With GOES-IR data, the west of the cloud cluster consisted of a long-lived mesoscale convective system (MCS) lasting about 36 h (Fig. 8). The major and minor axes of the MCS were about 400 and 300 km, respectively.

With Doppler radar data, the structure of the MCS was examined. The MCS moved to the west at a speed of 5 ms^{-1}, and a line-shaped rainband formed ahead of the MCS. The stratiform region is located on the eastern side of the line-shaped rainband (convective region) in the MCS. In the stratiform region, a mesoscale vortex at the middle level (from 3 to 8 km) was analyzed assuming that a system was steady (Fig. 9). The vorticity was 7.3×10^{-5} s^{-1} with a diameter of 323 km by a calculation with several assumptions.

The long-lived MCS with a developed line-shaped rainband in the west part of the cloud cluster moved westward after the cloud cluster decay. The cloud area of the MCS split at 00 UTC on July 3 and a newly developed convective area moved north and developed into the tropical cyclone over the Philippines. In other words, the tracked MCS was a system that developed into the tropical cyclone. Recent studies showed that a developed mesoscale vortex in MCS greatly contributed to the development of tropical cyclones. The characteristics of the mesoscale vortex (i.e., depth, horizontal scale, and vorticity) shown in this study were compared with those of previous studies, and the order of the vorticity was the same; that is, the observed MCS that developed into a tropical cyclone after 48 hours had a vortex in the middle troposphere. This study suggested the necessity to observe and track the mesoscale vortexes 48 hours before their development into the tropical cyclone.

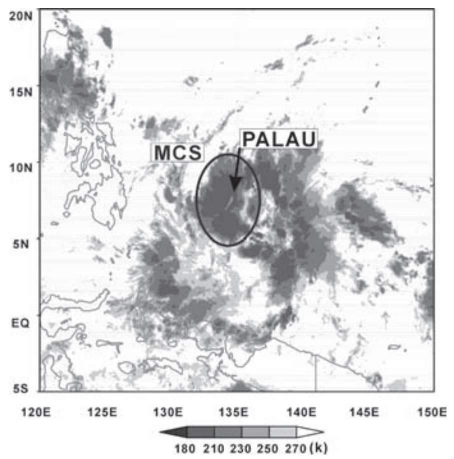

Fig. 8 GOES-IR image at 00UTC 2 July around Palau. The location of Palau is indicated by an arrow. The ellipse indicates the target MCS.

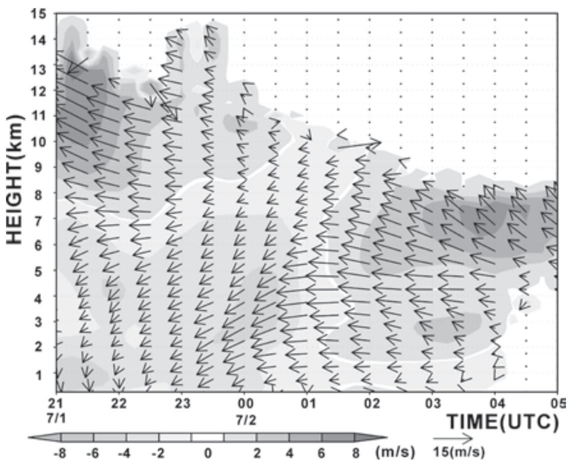

Fig. 9 Time-height cross section of horizontal wind (arrows) and their meridional component (shades) when the MCS passed.

The structure and formation process of the selectively developed snowband over the Sea of Japan in winter

For the purpose of understanding mesoscale winter snow storms, Nagoya University installed a dual Doppler radar system on the coast of the Sea of Japan from December 2002 to February 2003. On January 29, 2003, strong cold air moved over northern Japan and active snow clouds were observed over the Sea of Japan. On this day, during the period from 18 JST to 20 JST, the dual Doppler Radar system observed a selectively developed snowband whose echo-top height exceeded 5 km. The snowband was different from the disturbance associated with the Japan Sea Polar-airmass Convergence Zone (JPCZ), and the influence of geographical features and land breeze were not found. To reveal the structure and formation process of the developed snowband, we investigated the dual Doppler radar data and numerical simulation model CReSS.

From the Doppler radar observation, convective cells, which compose the snowband, developed both upstream and downstream of the snowband and lined up along the predominant wind direction and organized linear structure (Fig. 10). In the lower layer, west-northwesterly wind was observed on the north side of the snowband, while westerly wind was observed on the south side. A clear convergence line was formed along the snowband in the lower layer. In particular, at the downstream region of the snowband, the northerly inflow from a long distance was observed on the north side of the snowband and the low-level convergence was intensified. An enhancement of the low-level convergence contributed to the longevity of the convective cells that developed in the upstream region of the snowband and to the occurrence of convective cells in the downstream region of the snowband. Therefore, this played an important role in maintaining the linear structure of the snowband.

As a result of numerical experiments, when the snowfall system associated with the JPCZ began to decay, the corresponding snowband formed on the south side of the JPCZ. In the lower level, cold air was present in the southern edge of the snowband and high equivalent potential temperature air was inflowing from the north side (Fig. 11). Owing to the convergence of these airmasses, high equivalent potential temperature airmass was uplifted and formed convective cells. As a result, the snowband developed on the south side of the JPCZ. Furthermore, it is important to reach high equivalent potential temperature airmass to the south of the JPCZ. The snowfall system associated with the JPCZ should be in the decaying stage because the upper layer cold air was moving away from the Sea of Japan, and the stability of the atmosphere was increasing.

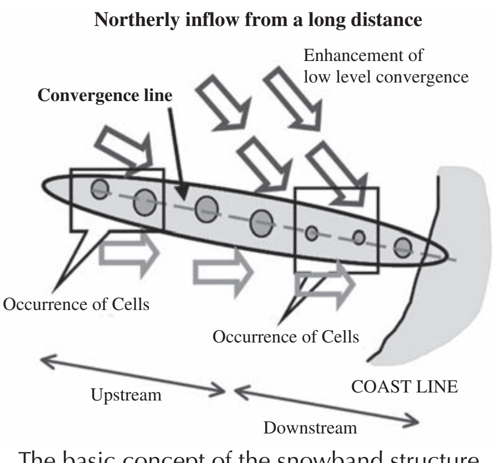

Fig. 10 The basic concept of the snowband structure shown by dual Doppler radar data analysis. Arrows show relative wind direction for the storm, and circles represent convective cells.

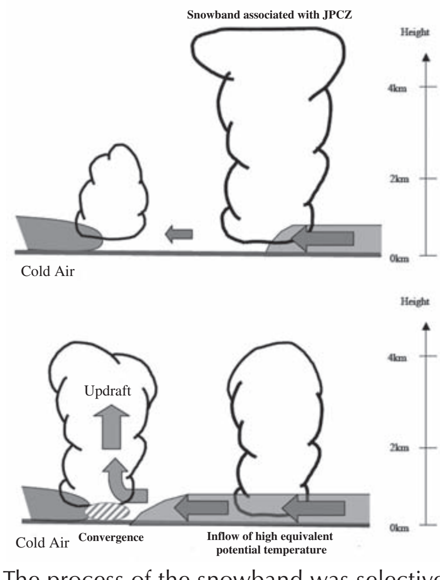

Fig. 11 The process of the snowband was selectively developed south side of the JPCZ. When the snowfall system associated with the JPCZ is in the decaying stage, high potential temperature air can reach the south side of JPCZ.

Development of the Lightning Simulator

We developed a Lightning Simulator that simulates charge distribution in thunderstorms and lightning on the basis of the Cloud Resolving Storm Simulator (CReSS).

Lightning activity of thunderstorms was simulated in two steps. The first step was the accumulation of electric charge by charging of cloud particles. The second step was discharge by lightning. In developing the Lightning Simulator, we introduced variables of charge as a prediction variable in the CReSS. First, we used the riming electrification: ice crystal, snow, and graupel that took charge in the microphysical process. Then, we described the formation of charge by riming electrification. Next, we calculated the electric potential and electric field from the charge distribution. We used the lightning parameterization that used the electric field as the threshold value of lightning initiation and parameterized discharge.

Thunderstorms that took lightning on the ground in summer formed the tripole structure of the charge distribution: the positively charged region in the upper layer, the negatively charged region in the middle layer, and the small positively charged region in the lower layer. We performed the ideal two-dimensional experiment to examine the reproducibility of the tripole structure of charge distribution within the riming electrification and lightning parameterization. The horizontal resolution was 500 m and artifactual sounding data were used as initial field. Simulated thunderstorms took the cloud-to-ground discharges and cloud flashes. The tripole structure of the charge distribution was formed in the model (Fig. 12).

Next, we performed a three-dimensional experiment of the thunderstorms developed over Aichi Prefecture of Japan on August 12, 2006. We compared the lightning strike points in the model with those observed by the Lightning Location System (LLS) operated by Chubu Electric Power Co., Inc. The horizontal resolution is 4 km and realistic environment data is used as the initial field. Although the timing and area of the lightning strikes were not exactly simulated in the model, we could reproduce the lightning strikes over the Aichi Prefecture with thunderstorms (Fig. 13). In this experiment, the Lightning Simulator could simulate the thunderstorm that took the lightning on the ground.

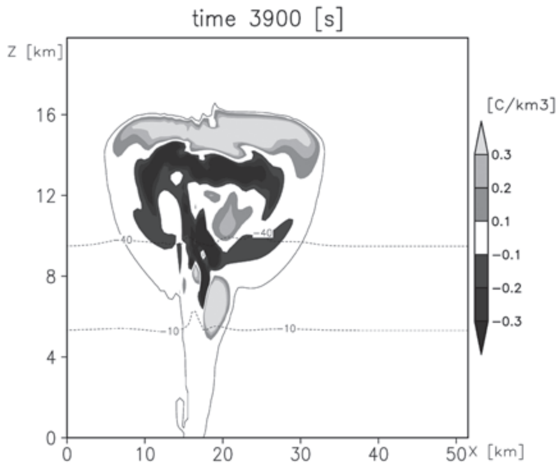

Fig. 12 A vertical cross section of total net charge of cloud water, rain, ice crystal, snow, and graupel at 3900 s. Shade represents net charge (C km^{-3}); solid line represents cloud border, and broken lines denote temperature (°C).

Fig. 13 Frequency of simulated lightning in three-dimensional experiment.

Laboratory for Climate System Study

Propagating diurnal disturbance embedded in the Madden-Julian Oscillation

Deep cumulus convection and heavy precipitation associated with the diurnal cycle over the Maritime Continent including the Indonesian Archipelago play an essential role in the Earth's climate system through a huge latent heat release. This world convection center is subject to the eastward propagating planetary-scale atmospheric disturbance called the Madden-Julian Oscillation (MJO), which originates over the Indian Ocean with a periodicity of about 30–60 days. Associated with the passage of a large-scale atmospheric disturbance, the modulation of the diurnal cycle over the islands has been observed. However, how the large-scale disturbance of the MJO modulates or is modulated by the diurnal cycle of convection/rainfall over the islands is not clear. Here, by using high-resolution TRMM precipitation data, we present the detail of actual rainfall activity that occurs under the large-scale MJO convection system. In this study, we investigated the MJO that propagated during the period from January to February 2001.

In order to elucidate the MJO space-time internal structure, the time-longitude diagrams of 3 hourly TRMM 3B42 rainfall averaged between 4°S–1°S during the end of January through February 2001, superimposed on the outgoing longwave radiation (OLR) (shaded) and zonal wind at 600 hPa (white contour), are shown in Fig. 1. Because the diurnal cycle was the most dominant mode in rainfall variability, a high-pass filter was applied to the data in order to extract the diurnal cycle component for TRMM rainfall data. The eastward propagation of deep convection (OLR) followed by the 600 hPa height westerly wind was apparent at a phase speed of about 3–4 m s^{-1}. Under the large-scale convection, the high-frequency variability in rainfall exhibited a significant eastward or westward propagation that is likely related to the background low-mid level wind. At the evolving stage of the MJO (end of January), aside from the standing oscillating rainfall over the western Indian Ocean (60°E), the westward propagating disturbances dominated to the west of the Maritime Continent (80°–120°E), intruding on the eastern Indian Ocean. Part of the westward propagating signal was triggered by each island and is associated with the diurnal rainfall over the islands.

In February, on the other hand, the eastward propagating diurnal disturbance (PDD) became pronounced over the whole Maritime Continent from the Indian Ocean to the Pacific as the center of the large-scale convection reached the major islands and the westerly prevailed. It should be noticed that the significant PDDs, which cut through the Maritime Continent from

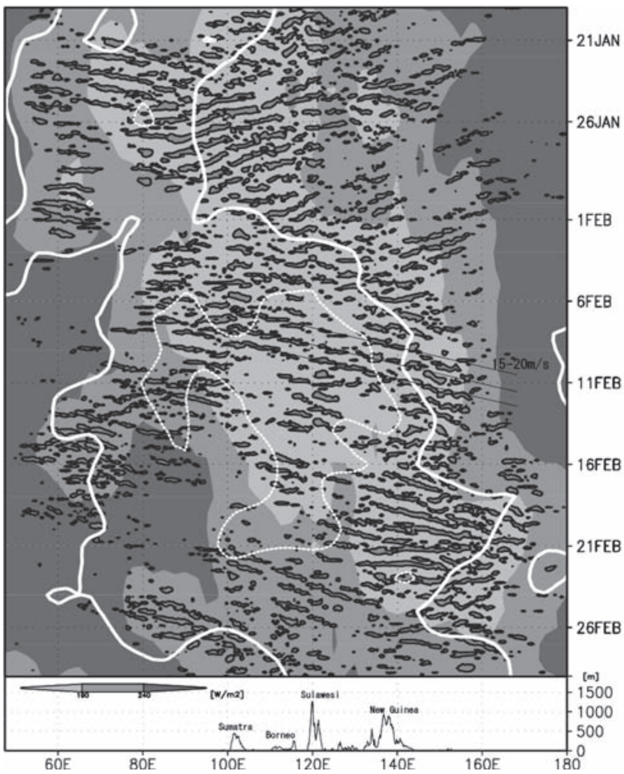

Fig. 1 Time-longitude cross section of the diurnal cycle filtered 3 hourly rainfall anomaly (contour: 0.2, 0.4 mm h^{-1}) are averaged between 4°S and 1°S from late January through February 2001. OLR (shaded) and zonal wind at 600 hPa (contour: solid, 2 m s^{-1}; dashed, 10 m s^{-1}) averaged between 5°S and equator are also described. The island terrain that averaged between 4°S and 1°S is denoted at the bottom. Black solid line corresponds to the penetrating diurnal disturbances (see text for details).

100°E to 160°E, appeared during February 6–11 (black solid line). The inferred phase speed of the propagating disturbances was about 15–20 m s^{-1}, which was close to the 600-hPa wind speed. These eastward PDDs are likely to play an important role in the propagation of the large-scale MJO convection. In association with the penetration of PDDs through the islands, the center of rainfall activity shifted from the western part of the Maritime Continent to the east. The PDDs, which started around 130°E–140°E and propagated toward the Pacific, became pronounced after February 16. On the other hand, the rainfall over the islands became rather scarce following the pervasive PDDs after February 10 between the significant rainfall over the Indian Ocean and the Pacific. The other noticeable feature is that the westerly area expanded eastward incrementally over the western Pacific in association with the eastward movement of the PDDs.

It is interesting to note that the timing of the PDDs (February 6–11, 2001) was consistent with a passage of the planetary-scale Kelvin wave (Masunaga et al. 2006) over the Maritime Continent. The dynamics of these PDDs across the Maritime Continent are not clear yet, but the penetration of the PDDs might be triggered by the large-scale equatorial wave as well as advection by the background westerly. Our results demonstrate that the diurnal cycle of convection over and around the major islands thus plays an active role in the propagation of the MJO over the Maritime Continent.

Role of the Tibetan Plateau and the Rocky Mountains in shaping the ocean climate in the North Pacific and North Atlantic

We examined the individual effects of the Tibetan Plateau and the Rocky Mountains on the ocean surface climate in the North Pacific and the North Atlantic using a coupled general circulation model (GCM-I) of the Meteorological Research Institute (MRI). For the summer anticyclone in the North Pacific, the Tibetan Plateau and the Rockies show comparable effects on the spatial features of pressure rise. However, in the eastern North Pacific, a relatively large rise in sea level pressure (SLP) occurs because of the Rockies. The Rockies create lower sea surface temperatures (SSTs) in the southeastern North Pacific than the Tibetan Plateau through air-sea interactions, such as a decrease in shortwave radiation flux to the ocean, increase in latent heat flux from the ocean, intensified upwelling, and cooler water transported from the north.

On the other hand, in the western subtropical North Pacific, an increase in SSTs due to the Tibetan Plateau is found year round and is particularly outstanding in spring. The enhanced winter subtropical anticyclone in the southeastern North Pacific due to the presence of the Tibetan Plateau creates ocean currents that transport warm sea water from the lower latitudes north to the western North Pacific. Therefore, SSTs in the western subtropical North Pacific increase because of the presence of the Tibetan Plateau. The higher SSTs in spring influence the summer surface climate of this ocean area, such as increasing precipitation. For these reasons, the zonal asymmetry of SSTs in the subtropical North Pacific is emphasized by the presence of both the Tibetan Plateau and the Rockies.

Figure 2 shows the ratio of the absolute value of the annual mean SST difference due to the Tibetan Plateau to that due to the Tibetan Plateau plus the Rockies, to present a spatial feature of the effect of the Tibetan Plateau contribution on annual mean SST differences. In the western North Pacific west of 180° along 20–30°N, a ratio above 0.7 was found, suggesting that the effect of the Tibetan Plateau was larger than that of the Rockies.

The presence of the Tibetan Plateau lowers SST in the lower latitude region of the North Atlantic by enhancing anticyclonic circulation that changes air-sea interactions; however, the Rockies do not have such an impact. The decrease in SST due to the Tibetan Plateau occurs notably in summer.

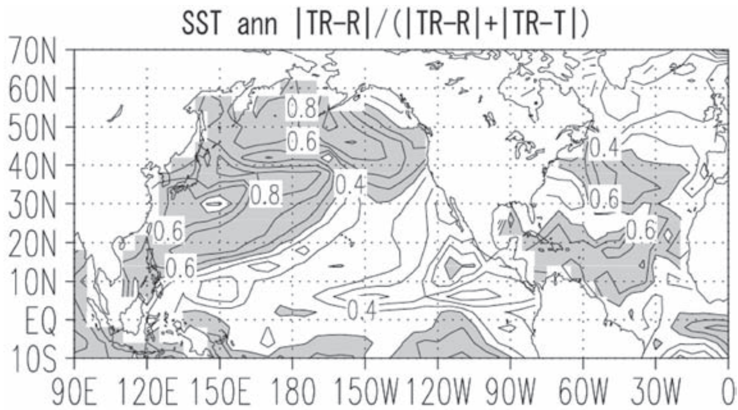

Fig. 2 Ratio of the absolute value of the annual mean SST difference due to the Tibetan Plateau to that due to the Tibetan Plateau plus the Rockies. The contour interval is 0.1, and the area above 0.5 is shaded.

Reference

Manabu Abe, Akio Kitoh, Tetsuzo Yasunari, and Osamu Arakawa: Role of the Tibetan Plateau and the Rocky mountains in shaping the ocean climate in the North Pacific and North Atlantic, *Climate Dynamics* (submitted).

Decreasing trend in rainfall over Indochina: Impacts of tropical cyclones

Recently, Intergovernmental Panel for Climate Change (IPCC) reported human-induced global climate change. Over the Indochina Peninsula, the long-term decreasing trend in rainfall was noted. Previous study suggested that the deforestation in northern Thailand induced the decrease in rainfall over Thailand. However, the decreasing trend in rainfall could be affected by the changes in large-scale circulation, which are unknown, resulting in human-induced climate change or natural variability.

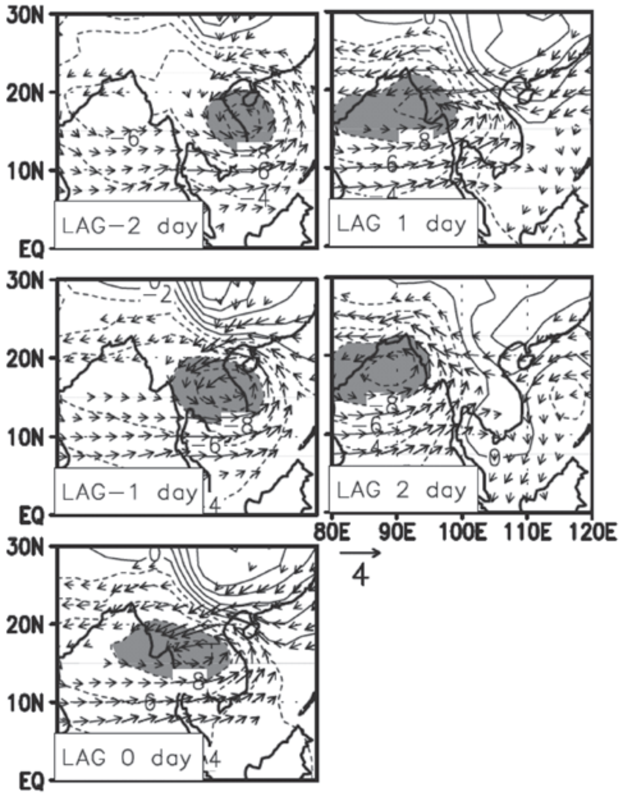

Fig. 3 Lag composite analysis of geopotential heights and winds anomalies at 850 hPa are shown. Based on daily rainfall over Thailand, 190 cases of high rainfall day (rainfall amount on a day exceeds 1 standard deviation from the mean) are selected. The anomalies were departures from the 43-year September mean of each variable. Gray shade shows that geopotential height anomalies are less than −8 gpm. The data is ERA-40 reanalysis derived by the European Centre for Medium-Range Weather Forecasting.

This study addressed a decreasing trend in rainfall during the late summer monsoon season (September) in Thailand from 1951 to 2000 and associated changes in large-scale circulations and tropical cyclone (TC) activity. Thailand receives significant rainfall during May to October and experiences two rainy peaks in late May to early June and September. Rainfall over Thailand in September was mainly brought by the westward propagating TC activity from the South China Sea and western North Pacific. The long-term trend in rainfall during the late summer monsoon season was closely associated with the number of landfalling TCs over the Indochina Peninsula. The change in the number of landfalling TCs over the Indochina Peninsula was likely caused by changes in the major cluster of TC tracks. Concurrent with the changes in TC tracks, the steering current of TCs was changed, which is likely to be associated with the strength of the subtropical high over the western North Pacific.

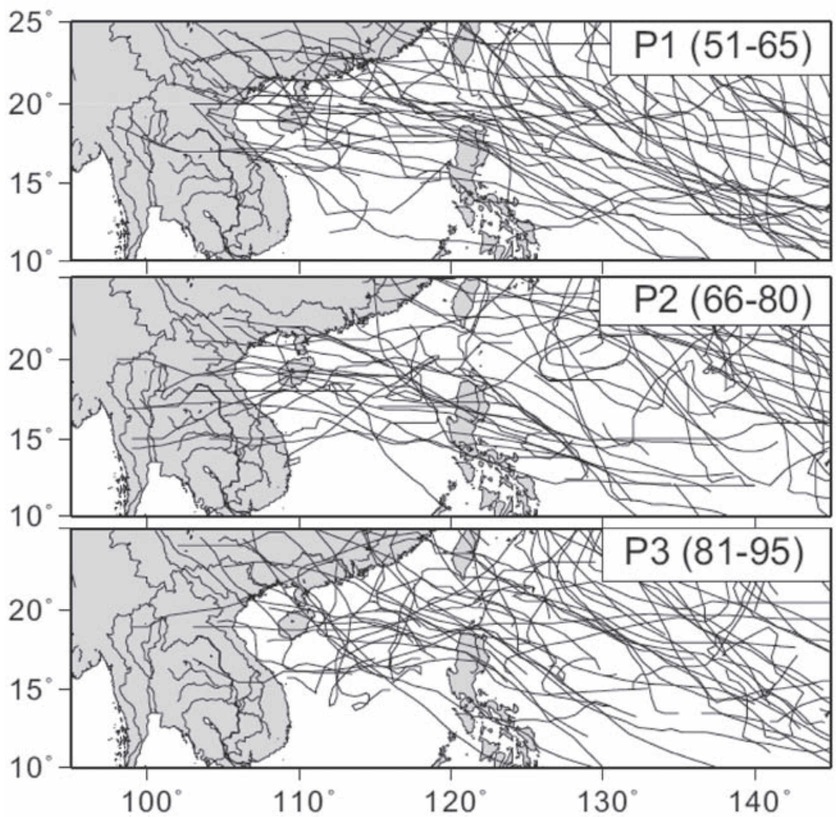

Fig. 4 Tropical Cyclone Tracks (derived from the Japan Meteorological Agency) in September in each period (P1: 1951–1965, P2: 1966–1980, P3: 1981–1995).

Laboratory for Cloud and Precipitation Climatology

Categorizing tropical rainfall based on satellite data

Precipitating clouds in the Tropics can be classified into different components in terms of cloud height and heaviness of rain. The most abundant component is shallow cumulus. Shallow cumulus does not reach the freezing level and produces moderate rainfall in the absence of frozen hydrometeors. Cumulus congestus grows to above the freezing level, yielding more rainfall than shallow clouds, although the cloud top is not as high as the tropopause. A deep convective core is a tall cumulus tower penetrating the whole troposphere, where rain drops melted from large ice particles (snow, graupel, and hail) created above the freezing level result in heavy rainfall. Deep convective cores are often surrounded by stratiform rain. Stratiform regions tend to be less turbulent and lower in rain rate than deep convective cores; however, they produce rainfall across a much wider area than convective cores do.

Figure 1 shows the joint histogram of precipitation height and cloud height analyzed from Tropical Rainfall Measuring Mission (TRMM) Precipitation Radar (PR) and Visible/Infrared Scanner (VIRS) infrared brightness temperature. The four storm categories of Shallow, Cumulus Congestus, Deep Stratiform, and Deep Convective are defined based on Fig. 1.

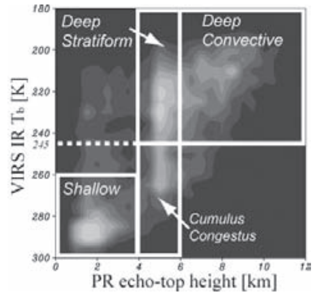

Fig. 1 Storm categories defined in the joint histogram of radar echo-top height and infrared brightness temperature (IR Tb).

Relative significance among the different storm categories varies with geographical regions, seasons, and El Niño Southern Oscillation (ENSO) phases. Time series of the probability of rainfall occurrence are plotted in Fig. 2 for different storm categories and for various tropical regions. Deep stratiform and convective systems are observed more often than shallow and cumulus congestus clouds in the West Pacific and Indian Ocean. In contrast, the shallow category is the dominant component most of the time in the Central Pacific. A key to understanding this regional contrast lies in large-scale ascent or subsidence (indicated by histograms). Deep stratiform and convective systems are commonly found in association with large-scale ascent (upward bars), while they tend to be overwhelmed by shallow clouds in the absence of strong ascent or under subsidence (downward bars). Deep systems can warm the surrounding atmosphere by latent heat release that works as a pump to generate large-scale circulation. The subsiding branch of the circulation caps the lower troposphere known as the planetary boundary layer (PBL). This cap, or the trade inversion, suppresses deep convective activity. It allows only shallow cumulus to barely emerge from the PBL. The storm categorization proposed here is useful for monitoring the variability of tropical precipitating clouds. Continuing research is underway to further deepen our climatological knowledge by applying the present methodology to longer-term data.

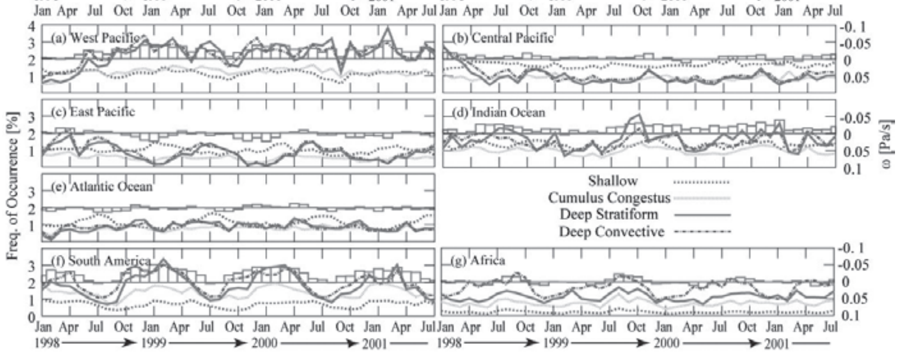

Fig. 2 Time series of the frequency of rainfall occurrence for different storm categories.

Observational study on the Madden-Julian Oscillation and tropical waves in the atmosphere

In the early 1970s, Roland Madden and Paul Julian discovered an eastward propagating mode recorded in weather station data over the Tropics. They named this mode “the 40–50 day oscillation” after its oscillatory period, which is now better known as the Madden-Julian Oscillation or MJO. The MJO has drawn increasing attention since it is the most outstanding component of tropical intraseasonal variability. Our understanding of the MJO has improved by many successful studies over the past 30+ years. Nevertheless, it would be fair to say that no single theory has succeeded in explaining every aspect of the MJO.

This study investigates the potential roles of the Kelvin and equatorial Rossby (ER) waves in MJO propagation by a composite analysis described as follows: The geographical center of MJO convection, hereafter called the base point (“x”s in Fig. 3), is first identified in each snapshot. Next, look east and west standing on the base point to find the Kelvin and ER waves, defined again by filtered outgoing longwave radiation (OLR) using proper bandpass filters. Repeating this procedure over 25 years of OLR data, a number of snapshots, longitudinally offset to the base point, are averaged together.

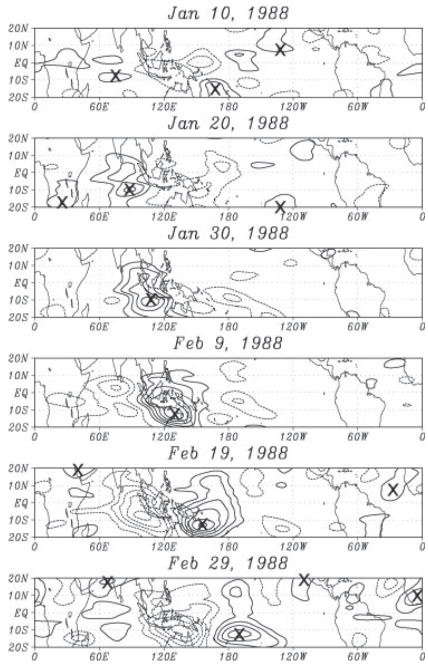

Fig. 3 An OLR-filtered MJO event. Solid (dashed) lines depict negative (positive) OLR anomaly.

Figure 4 shows a lag composite diagram for the austral summer MJO. The Kelvin wave (shaded) approaches from the west to the MJO convection center (or 0 in abscissa) prior to the MJO peak phase (or Day 0 in ordinate). The Kelvin wave finally arrives in the close vicinity of the MJO convection center on Day 0 and propagates further to the east once the peak phase has passed. In contrast, the ER wave (contoured), loosely concentrated around the 0 longitude for negative lags, exhibits little systematic pattern in the composite diagram. A comprehensive examination of multiple analyses including several case studies (not shown) suggests that (1) the Kelvin wave has an important role in MJO propagation and that (2) the interaction with the ER wave over the west Pacific warm pool leads to convective intensification, which gives rise to the peak phase of the MJO.

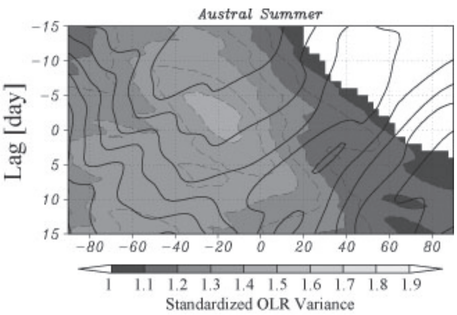

Fig. 4 The Kelvin wave (shaded) and ER wave (contoured) composited around the MJO convection center.

Satellite Data Simulator Unit

A crucial component of remote-sensing retrieval algorithms is radiative transfer simulation to synthesize satellite measurements. Computational schemes to solve radiative transfer problems are in general individually optimized to different kinds of sensors for practical reasons. Recent Earth observing satellites carrying multiple sensors, however, have led to increasing demands for a radiative transfer code applicable uniformly to different types of sensors. In response to such demands, we have developed the Satellite Data Simulator Unit (SDSU) for use by spaceborne microwave radiometers, radars, and visible/infrared imagers, which is available online from http://precip.hyarc.nagoya-u.ac.jp/sdsu/sdsu-main.html. Potential application of the SDSU package is not only limited to retrieval algorithm development but also includes cloud-resolving models (CRMs). It would help test and improve CRM performance to assess simulated measurements of various satellite sensors in comparison with actual observations.

Laboratory of Satellite Meteorology

Precipitation system study using satellite data

Satellite data are invaluable for a precipitation system study over a vast ocean. The Tropical Rainfall Measuring Mission (TRMM) satellite is equipped with a precipitation radar (PR), microwave radiometer (TMI), visible/infrared radiometer, and others. Originally TRMM was intended to study tropical rain systems. However, after more than nine years of operation, it was recognized that TRMM data are also useful for mid-latitude precipitation study. Here, so-called empirical orthogonal function (EOF) analysis was applied to the TMI signatures (Tb's) for the precipitation systems over the ocean near the Japan Islands.

The first principal function (EOF1) correlates with the near-surface rain rate due to emission from liquid water. All channels contribute equally to the variation except the 85.5-GHz channel in the summer case. This exception may be because summer precipitation is likely associated with the formation of many solid particles during the development of the system. The second EOF (EOF2) represents the amount of solid particles and also the near-surface rain rate. EOF2 largely varies with echo top height in summer and with both echo top height and freezing height in winter. EOF3 seems to represent the precipitation types.

This result suggests that the precipitation systems can be categorized by the microwave signatures. This categorization could improve the rain-rate estimation using microwave radiometers.

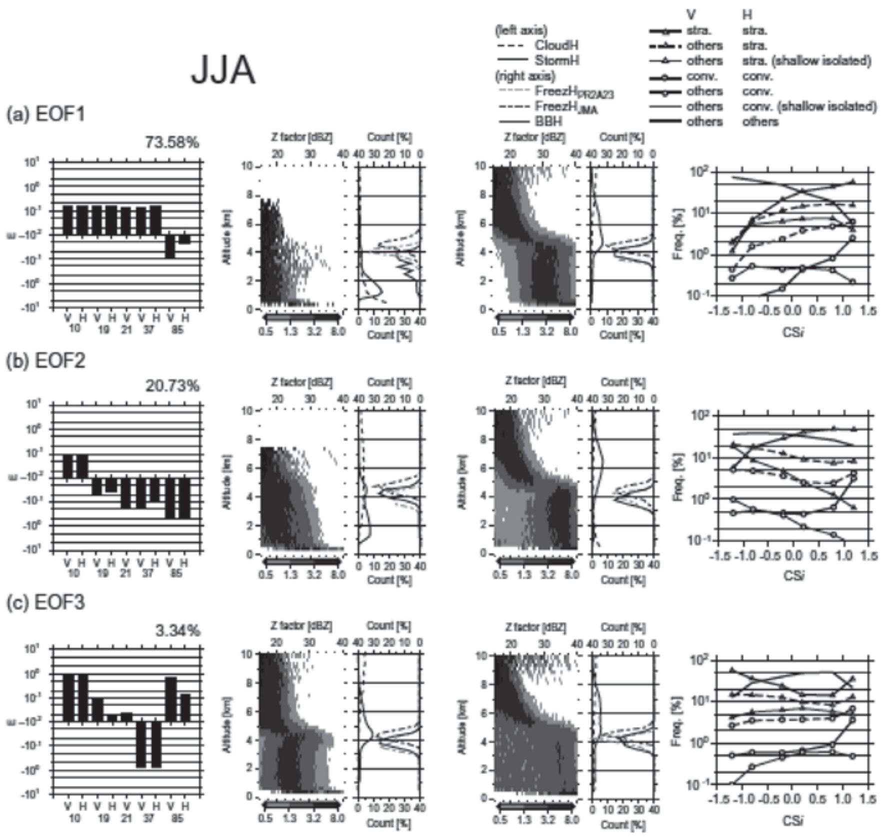

Fig. 1 Left-hand panels: Eigenvalues of TMI nine-channel Tb's and their percentiles of explained variance (the first column) in JJA. Center panels: CFAD of Z derived from PR 2A25 data (gray image, percentage every altitude), and histograms of the cloud top height (CloudH, dashed line), the rain height (StormH, solid line), the freezing height in 2A23 (FreezHPR2A23, thin dotted line), the freezing height in reanalysis data (FreezHGANAL, thick dotted line), and the bright band height (BBH, solid line) for EOFi-1.0 (the second column) and EOFi+1.0 (the third column). Right-hand panel: Frequency distribution of the precipitation types for each EOF.

Study on algorithms for new-generation space-borne precipitation radar

The Global Precipitation Measurement (GPM) is proposed as the successor to the Tropical Rainfall Measuring Mission (TRMM). The core GPM satellite will be equipped with a microwave radiometer (GMI) and a dual-wavelength radar (DPR). The combination of DPR and GMI data may improve instantaneous precipitation rate retrieval. The main objective was to improve DPR precipitation retrieval using GMI data. Discussion on the algorithm development strategy was continued. One of the important results is that the test data are essential. Several algorithms have already been proposed, but their advantages and disadvantages have not yet been fully investigated. Extensive test data including many extreme cases are required to clarify the characteristics of the algorithms. Ground-based measurement data, such as polarimetric Doppler radar data, wind profiler radar data, and disdrometer data, should be combined. Non-hydrostatic model results may also be incorporated.

Atmospheric boundary layer observation over Okinawa Island using a 400-MHz wind profiler radar

It is widely suggested that the south-southwesterly low-level jet (LLJ) is an important feature often accompanied with heavy precipitation events during the Baiu season in Japan and Mei-Yu in China. This link implies that a deeper understanding of the LLJ is necessary for studying Baiu precipitation. Data from UHF wind profiler observations during May–July over three years (2004–2006) are used to study the atmospheric boundary layer wind structure of the monsoon and the associated LLJ over Okinawa, a subtropical island in the Northwestern Pacific. Long-term observations of the wind with high temporal and vertical resolutions allowed us to investigate the LLJ statistical characteristics in detail. Hourly wind profiles are used for analyzing different LLJ categories. The result shows that the strong LLJ features are significant in the month of June over this island. The frequency of LLJ occurrence exhibits a diurnal cycle with a maximum in the early morning hours. The composition of three years of data also reveals that the southwesterly wind regime without rain has a clearer diurnal variation (Fig. 2). There is a trend of maximum wind propagating to a higher level in the afternoon hours. Such kinds of variations mostly occurred over a period of several days with strong surface heating, and the wind kept veering slightly with height and time.

This observation was conducted as part of a collaborative activity between HyARC and NICT.

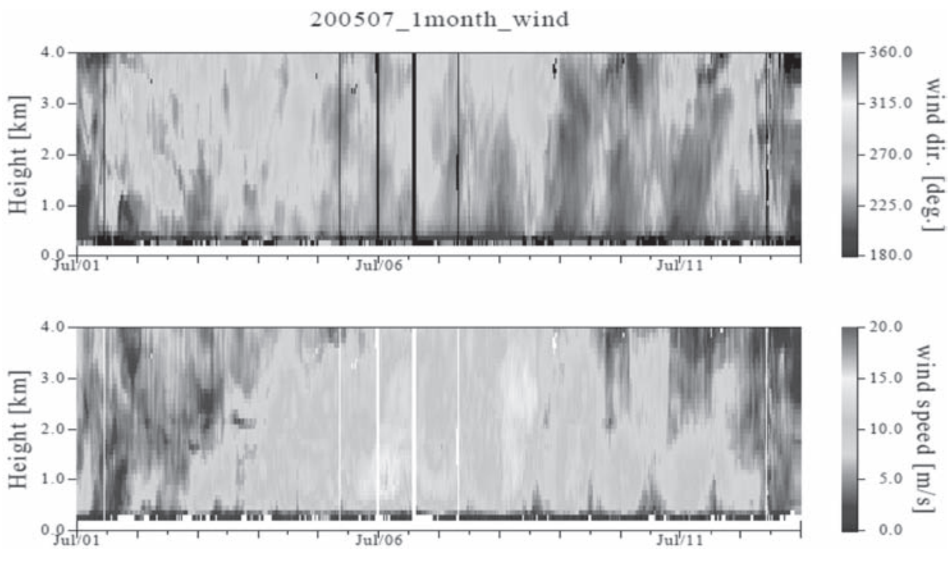

Fig. 2 Wind direction (upper) and wind velocity (lower) observed by a 400-MHz wind profiler radar at Okinawa Island during an intensive observation period in July 2005. The figure shows the clear diurnal variation of the wind.

Laboratory of Eco-Hydrometeorology

An interception loss experiment in a meteorologically regulated chamber

Interception loss (direct evaporation from the forest canopy) is very important to quantify the water budget estimation in a forested basin. The interception loss in forests is usually estimated from the difference between gross rainfall and net rainfall amounts above and below the forest canopy. The forest structure and some meteorological elements would affect the interception loss. However, it is difficult to reveal quantitatively how and what factors affect the interception loss in natural forests. Thus, in this study we tried to measure the interception loss using a regulated meteorological chamber with several experimental forests composed of young trees. The tree used in this study was boxwood of about 60 cm in height and about 30 cm in canopy diameter. We changed leaf area index (LAI) by cutting the branches and leaves and changing the stem density. We set steady meteorological conditions in the regulated chamber. We conducted the experiments at the Frozen Snow Disaster Prevention Experiment Ridge, Shinjo Branch, Snow and Ice Research Center, National Research Institute for Earth Science and Disaster Prevention. Figure 1 shows an example of experimental scenery, and Fig. 2 indicates arrangements of the experimental forests.

The meteorological settings were as follows: rainfall duration two hours, rainfall intensity 5.5 mm hr^{-1}, wind speed 0.5 m s^{-1}, air temperature 20 °C, and relative humidity 90%. After starting every experiment, the air temperature always decreased around 2 °C, and the relative humidity increased around 10%.

The relationships between interception rate and LAI or the stem density are shown in Figs. 3 and 4, respectively. Here the interception rate was estimated from the net rainfall amount above the forest canopy and the gross rainfall amount. It was shown that the interception rate increased with LAI regardless of the stem density (Fig. 3). On the other hand, clear relationships were not obtained between the stem density and the interception rate (Fig. 4).

Fig. 1 Experimental scenery.

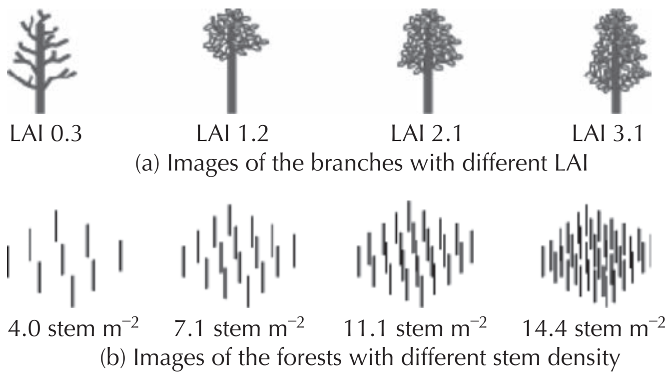

Fig. 2 Schematics of the experimental forests.

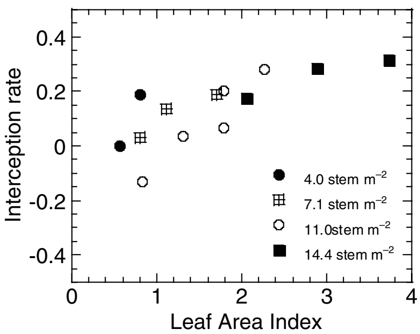

Fig. 3 Relationship between LAI and interception rate.

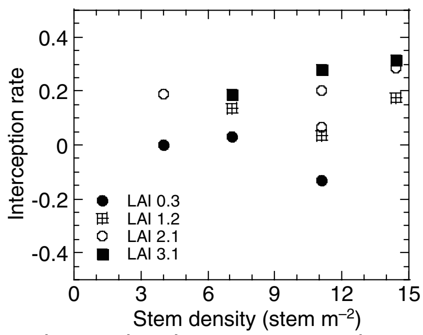

Fig. 4 Relationship between stem density and interception rate.

Characteristics of atmospheric turbulence spectrum above the forest canopy under stable conditions

Because forests have large roughness to the atmospheric flow, the roughness sublayer (RSL) is formed above the ground up to 2–3 times higher than the mean tree height (h). Turbulence structure in the RSL tends to be different from that in the atmospheric surface layer (ASL). Although understanding the turbulence structure under various conditions is essential for accurate estimation of the exchange of momentum, heat, and mass between forests and the atmosphere, the knowledge under stable conditions is not well known. Thus, this study investigated the turbulence spectrum under stable conditions using 10 Hz data obtained by ultrasonic anemometer thermometers (Solent R3 ; Gill Inst., Ltd., UK), which were installed two heights above a larch forest growing on flat terrain (42°44’N, 141° 31’E; Tomakomai Flux Research Site managed by National Institute for Environmental Studies). The observation was conducted from June to October in 2002, and data for this analysis were selected to satisfy a 30-minute stationarity. To reduce random spectrum errors, ensemble averaging was done after classifying all 30-minute spectra by atmospheric stability (ζ).

Figure 5 shows velocity and temperature spectra and momentum and sensible heat cospectra obtained at two heights above the canopy under stable conditions. For every variable, the spectrum exhibited a sharper peak compared to the ASL spectrum obtained from previous studies. Furthermore, the peak shifted toward lower frequencies, with a few exceptions of momentum cospectrum under weakly stable conditions. These findings revealed the existence of large coherent eddies initiated by wind shear around the canopy even under stable conditions, though it was usually observed under near-neutral conditions.

Such spectral characteristics were conspicuous in streamwise wind velocity and temperature spectrum. Because their peak frequencies were observed at lower frequencies than that of vertical wind velocity, representing fluctuations attributed to wind shear near the surface (active motion), it was suggested that they were affected by fluctuations attributed to the large atmospheric field over the forest (inactive motion). Furthermore, the similar peak shape and frequencies in momentum and sensible heat cospectra to those of streamwise wind velocity and temperature spectra suggest that the inactive motion accounts for vertical transfer above the forest canopy to some extent.

The observed spectra of all variables showed the tendency to approach the ASL spectra with increasing stability. Especially for the spectra of vertical and lateral wind velocity and the cospectra of momentum and sensible heat flux observed at the upper level, the second peak appeared at frequencies close to the peak frequency of the ASL spectrum. The existence of double peaks must indicate that RSL turbulence consists of coherent eddies and ASL turbulence. The results suggest that RSL height decreased with increasing stability, and consequently the effect of ASL turbulence was relatively intensified.

Challenges for the future are to investigate the RSL spectrum for the general applicability of the stability dependence obtained by this study. The relationship between the peak frequency of the RSL spectrum and surface parameters, such as mean tree height and vegetation density, should also be studied.

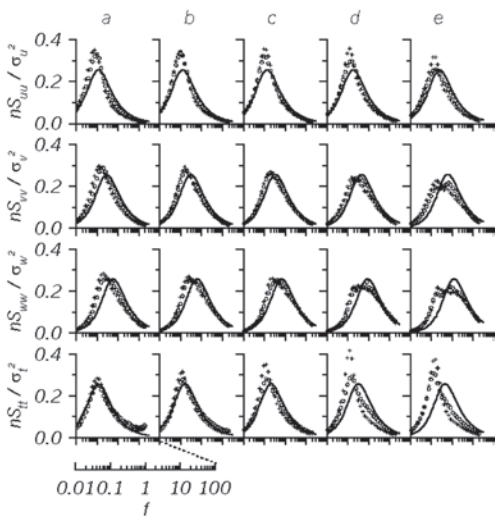

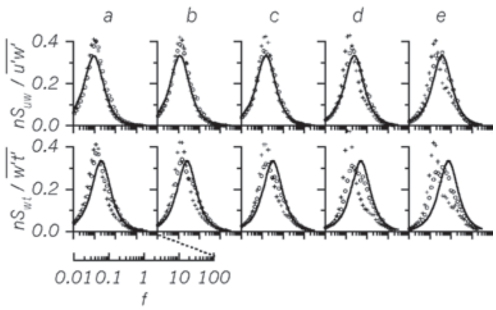

Fig. 5 Longitudinal axis represents normalized frequency f (= n z/U; n: frequency, z: measurement height, U: mean wind speed) and vertical axis shows frequency-weighted power spectra and cospectra normalized by variance or covariance (u: streamwise wind velocity, v: lateral wind velocity, w: vertical wind velocity, t: temperature, uw: momentum flux, wt: sensible heat flux). Data were obtained at 1.7 *h* (open circles) and at 1.2 *h* (crosses). Appended solid lines represent the empirical models for the ASL spectra. The alphabets above the figure indicate the category of ζ (a: 0.02–0.04, b: 0.08–0.1, c: 0.15–0.2, d: 0.4–0.5, e: 0.8–1).

Laboratory of Ocean Climate Biology

The climate system surrounding us is governed by cycles of water and materials in the hydrosphere and atmosphere on Earth. In this laboratory, we study the inter-relationship between climate change and ocean biogeochemistry on time scales ranging from a decade to a century. Brief description of our laboratory activities follows.

● Ocean Primary Production Monitoring by Satellites

Primary production is one of the key processes in understanding the relationship between climate change and ocean biogeochemistry. A global view of the primary production can be attained by satellite remote sensing, but the quantitative estimation of primary production is still hindered by the lack of *in situ* data to validate the satellite observations. To fill this gap, we developed an underwater profiling buoy system and a custom made fast repetition rate fluorometer (FRRF), and constructed an ocean primary productivity profiling system. This work was done as a part of the Core Research for Evolutional Science and Technology (CREST) program 1999-2004. Currently, we are developing a pilot system to monitor oceanic primary production by combining the productivity profiling system in operation with supporting data handling systems to merge satellite and *in situ* data. This work is being conducted under a new 5-year continuation project as part of Solution Oriented Research for Science and Technology (SORST) program, started in 2004. The goal of the project is to design a practical system to monitor the global ocean primary production. The immediate tasks are to validate the satellite primary production data, and to demonstrate the usefulness of the validated satellite data for studies of the temporal and spatial variations of ocean biogeochemistry in response to the physical forcing functions at the surface ocean. [In this text, the term "primary productivity" is used for rate of "primary production" in time scale of an hour or a second. The term "primary production" is used conventionally for the "primary productivity" in time scales of a day or a year.]

Operation of ocean productivity profiling system in the western subarctic North Pacific

The underwater profiling buoy system developed in collaboration with Nichiyu-Giken Co. Ltd. is composed of an underwater winch system and a profiling buoy system. The profiling buoy is equipped with sensors and normally stays below the euphotic zone. Profiling measurements are done in the upper layers from the winch depth to the surface according to a preset schedule. We installed a custom made FRRF (KIMOTO Electric Co. Ltd.) as a main sensor, in which the data processing is conducted in real time during the profiling measurements. All the measurement data are stored and a part of the processed data is transmitted to the laboratory via cellular phone before the buoy sinks back to the resting position.

During the period from June 9 to July 15 2006, we deployed the ocean productivity profiling system at a station in the western subarctic North Pacific (47°50'N, 160°00'E: 5115m of depth). That was the first offshore mooring in deep water. Out of 39 scheduled operations, 34 profiles were obtained successfully with 22 completed real time data transmissions. Data collected from the system are shown in Fig. 1. In late June, both the chlorophyll *a* concentrations (Chl *a*) and gross primary productivity (GPP_c) dropped (Fig. 1b, c), probably because of the intrusion of different (other) water masses. On the other hand, the biomass specific gross productivity ($GP^b{}_c$) increased (Fig. 1d). In the same period, dissolved oxygen remained oversaturated and acoustic backscattering strength data of ADCP showed an increase in large particles that did not contain chlorophyll *a* within the upper layer. These data implied that grazing pressure of zooplankton on phytoplankton was probably a principal controlling factor of primary productivity. This is the first-ever *in situ* measurements of the open-ocean productivity in such high time resolution, demonstrating the utility of the monitoring system in further understanding the natural variability of ocean productivity.

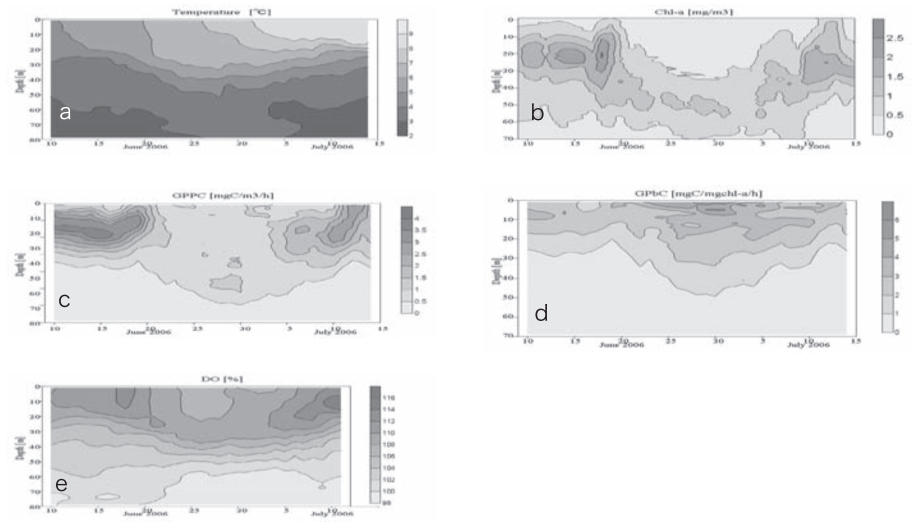

Fig. 1. Time series data transmitted from the monitoring system in the western subarctic north Pacific from June to July 2006. (a) Temperature, (b) Chl *a*, (c) gross primary productivity (GPP_c), (d) Chlorophyll *a* specific gross productivity ($GP^b{}_c$), and (d) dissolved oxygen saturation (%).

Estimation of oceanic daily depth-integrated primary production from FRR fluorometry

In the operation phase, the ocean productivity profiling system conducts a few FRRF measurements per day, which provide depth-profile data of instantaneous chlorophyll *a* specific primary productivity ($P^B{}_{O2}$). In order to validate satellite derived production, daily depth-integrated production (mgC m^{-2} d^{-1}) needs to be estimated. In this study, we constructed an algorithm to estimate daily depth-integrated production from a single FRRF observation, using a database obtained from intensive FRRF measurements in the Sagami Bay from 2003 to 2006. This analysis reveals that FRRF-based hourly $P^B{}_{O2}$ is mainly controlled by σ_{PSII} (effective absorption cross section of PS II for phytoplankton) (Fig. 2b) at a high irradiance level where Φ_e (quantum yield of electron transfer for O_2 evolution) was below the theoretical maximum, 0.25 (Fig. 2a). Using the midday FRRF data, we determined a threshold of underwater-PAR ($E_{\Phi e}$) where Φ_e <0.25, and derived distinct empirical relationships for two cases of underwater PAR (E) level. For $E>E_{\Phi e,}$ the E-σ_{PSII}, and σ_{PSII}-$P^B{}_{O2}$ relationships are incorporated into the new algorithm, and for $E<E_{\Phi e,}$ the E-$P^B{}_{O2}$ relationship (Fig. 2c) is used. By applying the estimated time series profile of E to the empirical relationships, we calculated the time series profile of $P^B{}_{O2}$. Finally, the profile was multiplied by the Chl *a* and integrated over depth and time, to estimate daily depth-integrated production (mmolO_2 m^{-2} d^{-1}) was estimated. The algorithm-derived production showed good agreement with measured ones (Fig. 2d), and thus the estimation of near-surface production was greatly improved.

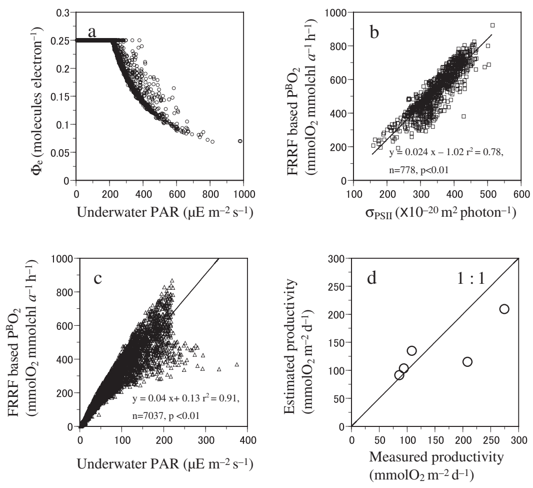

Fig. 2. Relationship between (a) underwater PAR and Φ_e, (b) $P^B{}_{O2}$ and σ_{PSII}, (c) $P^B{}_{O2}$ and underwater PAR, and (d) comparison of daily depth-integrated production between intensive FRRF measurements and algorithm-derived estimates in Sagami Bay.

Plankton metabolic balance in the upper ocean

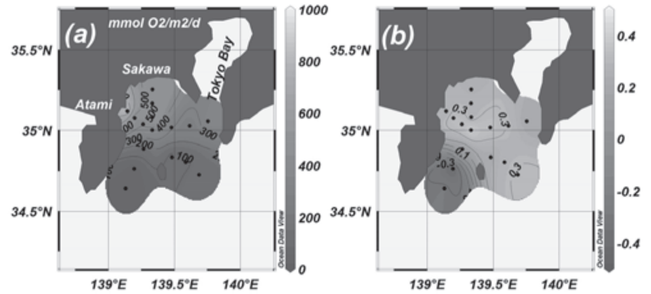

Fig. 3. Spatial distribution of (a) GPP and (b) NCP/GPP ratios in Sagami Bay during May 2006.

When we consider the functional role of an ocean ecosystem, it is critical to determine the spatial variability in the net metabolic status and the balance between gross production and community respiration in a given oceanic ecosystems, because it would dictate whether oceanic regions are net sources or net sinks of CO_2 to the atmosphere. In this study, we measured the time (7-10 days) and depth integrated plankton metabolic rates of gross primary production (GPP), net community production (NCP) and community respiration (CR) using triple oxygen isotopes and O_2/Ar ratios with our recently developed high-resolution spatial underway sampling technique, in Sagami Bay during May 2006. The estimated GPP varied from 34 to 963 mmolO_2 m^{-2} d^{-1} in the mixed layer and higher production rates were observed in the eutrophic coastal regions around the head of a bay (Fig. 3a). The NCP/GPP ratios in the Sagami Bay varied from –0.5 to 0.3. The higher ratios were observed in the southeastern Bay (0.17 to 0.3) and the lowest ratios in the southwestern Bay (–0.49 to 0.09), whereas they were between 0.07 and 0.26 in the rest of Sagami Bay (Fig. 3b). The negative NCP/GPP ratios in the southwestern open sea region indicate that community respiration was dominant over the production during the study period. Our study suggested that coastal regions showed strong autotrophy whereas heterotrophy was observed in the offshore regions: also as a whole, plankton production is slightly in excess of community respiration. This excess carbon can support the export of carbon to the oceans' twilight zone.

Seasonal and diel variations in heterotrophic bacterial community in Sagami Bay, Japan

Bacteria utilize dissolved organic carbon (DOC), incorporate it into particulate biomass, and thereby help mediate cycling of nutrients and materials in seawater. For constructing a model of oceanic net metabolic balance, it is important to understand mechanisms regulating the abundance of heterotrophic bacterioplankton. In this study, natural populations of bacteria were sampled from Sagami Bay in April, June, and August 2004, stained with DNA-specific fluorochrome SYBR Green I, and analyzed by flow cytometry. The mixed layer temperature progressively increased through the study period from 17°C in April to 27°C in August whereas the salinity decreased from 34 to 33 exhibiting the onset of stratification from April. The Chl *a* was highest in April followed by June and August. The bacterial population showed a similar seasonality, indicating that it is primarily controlled by the supply of DOC via phytoplankton's photosynthesis. Also positive correlations were significant between diel changes in bacterial abundance and Chl *a* during each study period (Fig. 4). In June, however, the bacterial abundance was occasionally low despite the high Chl *a*, which is probably due to grazing by bacterivores.

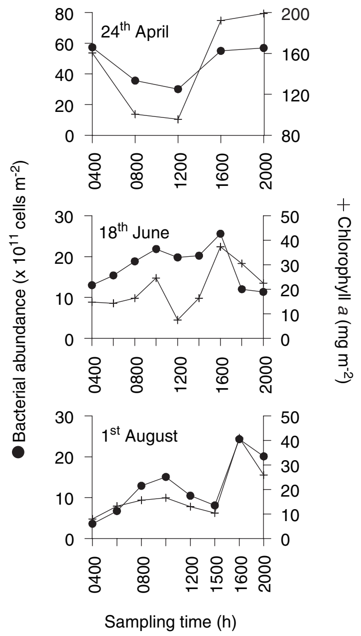

Fig. 4. Diel variations in bacterial abundance and Chl *a* in Sagami Bay during the study periods.

Effect of biofilms on the performance of fast repetition rate fluorometer (FRRF)

As with any substratum immersed in seawater, sensors are susceptible to "Biofouling" which is caused by the adhesion of micro- and macro-organisms, and can diminish sensor operation and performance. To achieve long-term monitoring of ocean primary production using the ocean productivity profiling system, the biofouling effect on FRRF data during deployment should be determined. Here, we examined the effect of biofouling on the performance of FRRF (Chelsea Instruments Co. Ltd.) with simulation experiments in which measurements were made by placing fouled coupons of different levels of biofilm transmission and Chl *a* on the FRRF excitation and detection windows. Our results showed that the biofilms dominated by chlorophyll *a* containing organisms on the detection window affected the quality of fluorescence data; the F_0 and F_m values increased and the potential photochemical quantum yield of PSII (Fv/Fm) decreased accordingly (Fig. 5). This is because the detection window received fluorescence signals not only from the sample algae but also from the chlorophyll *a* in the biofilm, which was excited using an LED flashlight. It was observed that Chl *a* greater than 0.3 mg cm^{-2} in the biofilm on the detection window would critically affect fluorescence measurements. On the excitation window, the biofilm reduced the flash intensity; this also affects the data quality only if transmission is significantly reduced. These observations suggest that the fluorescence data would be disturbed by biofouling on the optical windows, especially with the case of biofilm containing chlorophyll *a* on the detection window. However, with the biofouling effect quantified in this study and the measurement of Chl a on the detection window it is possible to correct the FRRF data if the flash intensity remains nearly constant during deployment.

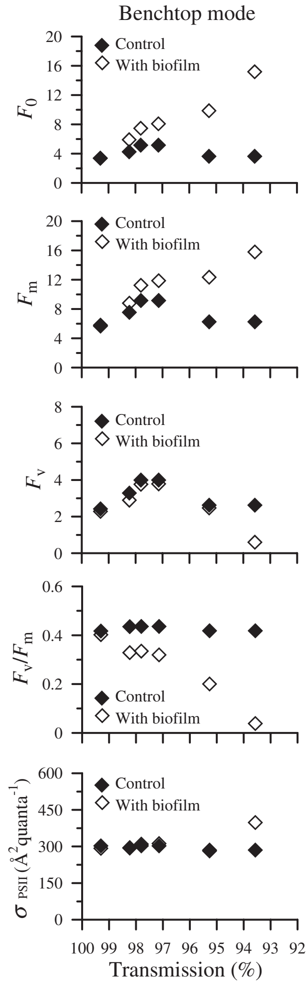

Fig. 5. Effects of natural biofilms (placed on both of the FRRF optical windows) on FRRF measurements made in bench top mode. Note: Units of F_0, F_m, F_v and F_v/ F_m are dimensionless.

Diel variations in photo-physiological state of phytoplankton assemblages in the upper Gulf of Thailand

In coastal seas relatively high primary production occurs because of the supply of land-driven nutrients, accounting for about 1/5 to 1/3 of the global ocean production. The coastal primary productivity has large variability, both in time and space, in response to changes in environmental conditions caused by tidal movements, river inflow, and human activities. In this study, we conducted intensive FRRF observations (2 hr interval from 8:00 to 18:00) in the upper Gulf of Thailand (UGOT) in July 2006, to evaluate a diurnal change in the photo-physiological state of natural phytoplankton assemblages. Here, we report the result of FRRF-based photosynthetic parameters, the potential photochemical quantum yield of PSII (F_V/F_M), and the effective absorption cross-section of PSII (σ_{PSII}), obtained from the eastern and western sites of the UGOT (Stn. 1 and Stn. 5, respectively). At Stn. 1 where the salinity stratification had developed because of river inflow, σ_{PSII} and F_V/F_M range from 340 to 820

Å^2 photon^{-1} and from 0.4 to 0.6, respectively. In the well-mixed waters of Stn. 5, they range from 480 to 900 Å^2 photon^{-1} and from 0.2 to 0.6 (Fig. 6). A significant decay of σ_{PSII} observed in the upper layer during the day is correlated with underwater PAR increase, indicating that phytoplankton get acclimated to high light condition (Photo acclimation) by reducing their light harvesting ability to circumvent photo-damage. On the other hand, a negative correlation of F_V/F_M to PAR is found in Stn. 5, indicating that parts of the photosynthetic unit of phytoplankton would be damaged by high light (photo-inhibition). This is probably because in Stn. 5, the low-light adapted phytoplankton were dominant because vertical mixing causes exposure to a broad range of light levels.

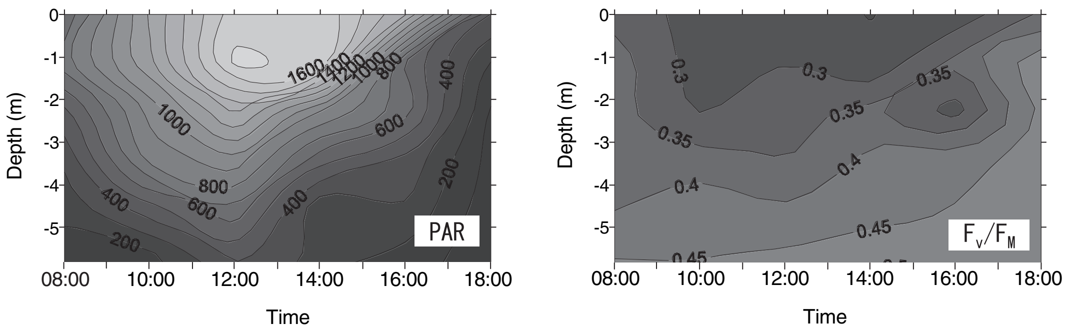

Fig. 6 Diel variations in under water PAR and the potential photochemical quantum yield of PSII (F_V/F_M) in the western site (Stn. 5) of the upper Gulf of Thailand.

• Studies on changes in the biogeochemical cycle in oceans with reference to climate change

Estimation of gas exchange coefficient (piston velocity) using stable oxygen isotopes

The accurate estimation of the transfer of trace gases across an air-water interface is required to understand the ocean-atmosphere coupling of the biogeochemical cycle in the earth system. Although a variety of different parameterizations were proposed to calculate the gas exchange coefficient (K) using different models and different tracers, the use of these parameterizations led to K values that could differ by a factor greater than2. Accordingly, these estimates have large uncertainties (~30%) resulting in large errors in the flux estimates. We estimated K by a novel method using triple oxygen isotopes in dissolved O_2. This method relies on an observed isotopic anomaly for molecular oxygen in seawater. The $\Delta^{17}O$ anomaly in the mixed layer is controlled by gross oxygen production (GOP) and influx of O_2 from the atmosphere. In this study, we measured changes in the $\Delta^{17}O$ anomaly in the western subarctic North Pacific during night-time, when no GOP occurs, at every 2 hr interval for four nights during July to August in 2006. The piston velocity derived from the $\Delta^{17}O$ anomaly was consistently higher at lower wind speeds and similar at higher wind speeds compared with that of Wanninkhof and McGills (1999) (Fig. 7). Relative to other methods, the present method is more robust and gives a K value in the semi-diurnal scale with reduced errors. Therefore, it is possible to estimate daily variations in K using this method, leading to a more precise estimation of air-sea flux of carbon.

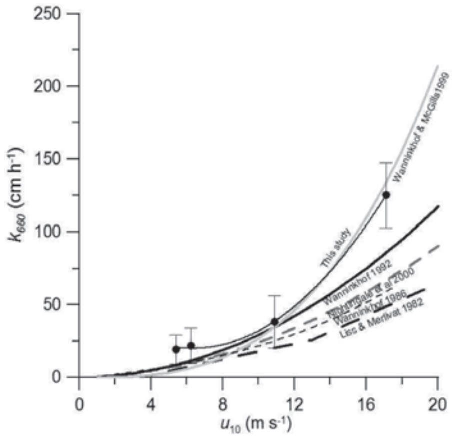

Fig. 7. Wind speed versus piston velocity of oxygen – comparison of the $\Delta^{17}O$ anomaly model with other models.

Impact of the bi-weekly tidal variations on Chl *a* in the northwestern Okhotsk Sea, central Kuril, and Aleutian Islands areas

In the subarctic North Pacific, the high Chl *a* for the post-spring bloom period (late summer) are commonly confined to dynamically active zones (straits, banks, etc.), where nutrients are supplied to the euphotic layer. Because of the superposition of K1 and O1 tides, the tidal current speeds in the northern Okhotsk Sea, Kuril, and Aleutian Islands regions are undergo significant bi-weekly variations. Using satellite-derived Chl *a*, PAR, and sea surface temperature data, we have examined the temporal variability in Chl *a* in response to bi-weekly tidal variability. Our results show that temporal changes in the spatially averaged Chl *a* in the surface waters of central Kuril and Aleutian Islands regions are induced by quasi-periodic (period of 6-9 days) variability in PAR, bi-weekly variability in tides (Fig. 8), and water exchange between the inshore and offshore areas forced by anticyclonic eddies. In the northwestern Okhotsk Sea (Kashevarova Bank region), the enhanced tidal mixing increases Chl *a* during high PAR and high phytoplankton biomass period and reduces Chl *a* during low PAR and low phytoplankton biomass period. For the Kuril Islands area, we observed an increase of the spatially averaged Chl *a* in the surface waters during moderate tides (Fig. 8). It can be related with an increase of the phytoplankton growth in the surface waters due to nutrient and biomass supply from the subsurface (the Chl *a* maximum layer) to surface layers. During strong tides the Chl *a* was significantly reduced (Fig. 8), probably because the average light energy available to phytoplankton cells was reduced, and the tides resulted in increased phytoplankton losses because cells were removed from the surface layer.

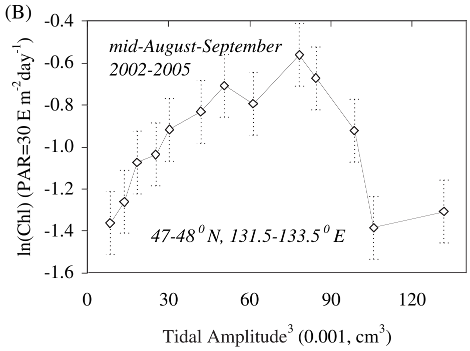

Fig. 8. Log Chl *a* (adjusted to PAR=30 E m^{-2} day^{-1}) versus tidal amplitude in Kuril Islands area.

Chl *a* response to autumn wind events in the coastal northern Japan Sea

The northern Japan Sea has many characteristics of subarctic waters, with large seasonal variability reinforced by a monsoon climate. In the coastal waters, northwest wind-driven upwelling supplies abundant nutrients to be processed by phytoplankton production in autumn. To understand such wind-driven effects on the primary production, we analyzed satellite Chl *a*, sea surface temperature (SST), and PAR data collected between 1997 and 2006. In the study area (Fig. 9a), the Chl *a* increased from ~0.8 μg L^{-1} in September to ~2.0 μg L^{-1} in November while daily PAR decreased from ~35 E m^{-2} to ~17 E m^{-2}. The spots of high Chl *a* were related to upwelled waters identified by low SST. Our results show a strong correlation between Chl *a* and strength of the wind induced upwelling in the coastal area (Fig. 9b). Enhanced upwelling leads to a shallower pycnocline layer (characterized by high nutrients and seed stocks of phytoplankton cells) and thus promotes photosynthesis in the sea surface as phytoplankton responds to high light and nutrients.

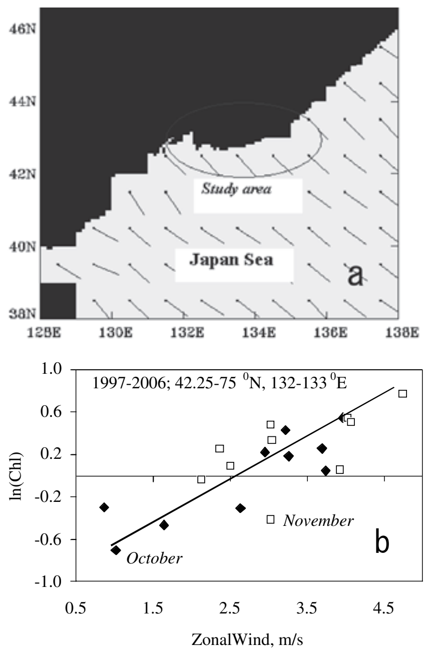

Fig. 9. (a) Study area and wind stress vector (November 1997-2006), (b) Log Chl *a* vs. zonal wind.

Spatial distribution of $\delta^{15}N$ of suspended particles in the surface waters of Sagami Bay

The downward transport of carbon via the “biological” pump plays a major role in the CO_2 sequestration to deep oceans. In general, the biological pump is expected to be enhanced in highly productive periods (such as spring blooms); however, the regulating mechanisms of the biological pump efficiency remain unclear. Here, we examined spatial variations in $\delta^{15}N$ of the sea surface suspended particles ($\delta^{15}N_{sus}$) in Sagami Bay during May 2006 to understand the properties of nutrients drawdown resulting from phytoplankton production during winter to spring transition. The $\delta^{15}N_{sus}$ ranged from 4.6 to 8.9 per mil and correlated negatively with the silicate to phosphate (S_i/P) ratios of dissolved nutrients concentrations (Fig. 10). This implies higher contribution of diatom to the integrated nutrients drawdown (f_{Diatom}) in the regions where the efficiency of nutrient consumption by phytoplankton (= consumption/nutrient supply; U) is high. The analysis of $\delta^{15}N_{sus}$ with a simple Rayleigh Distillation equation demonstrates positive relationships of f_{Diatom} (0.2-0.7) to U (0.4-0.7), and the integrated phosphate drawdown (0.14-0.42 μmolP L^{-1}). These results emphasize a significance of the diatom group in the nutrients drawdown, and thereby emphasize the biological pump efficiency during productive seasons in Sagami Bay.

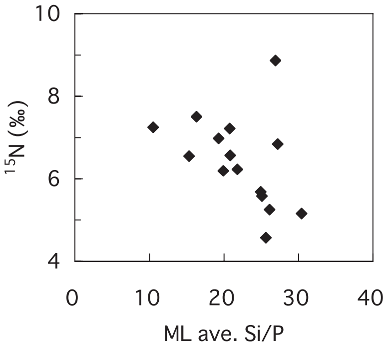

Fig. 10. Relationship between mixed layer averaged Si/P and $\delta^{15}N_{sus}$ of suspended particles in the surface waters of Sagami Bay in May 2006.

Particle dynamics in the subsurface Sagami Bay

Organic matter produced in the euphotic zone of oceans sinks down to deeper layer as particles. They are consumed by organisms and decomposed via biological processes in the water column. Although the biological activities are relatively higher in the near surface layers, little is known about the particle dynamics such as production, transformation, and decomposition in and/or during transport out of the upper oceans. In this study, we examine the vertical changes in ^{13}C and ^{15}N characteristics of suspended and sinking particles in the upper water column of Sagami Bay to articulate the processes in particle dynamics within the surface-subsurface layer. The sinking particles were collected by a set of multilayer traps at 20-140m (7 layers, 20 m intervals), moored at the central part of the Bay from May 2 to 9, 2006. Trapped materials were separated into two fractions, one the “small sinking particles” (<20 μm), and the other “large sinking particles” (>20 μm). Isotopic measurements were made for each fraction. Our result reveals that almost all the sinking particles consist of “large sinking particles” which showed little variation in $\delta^{13}C$, $\delta^{15}N$, and C/N ratios with increasing depth (Fig. 11). These properties are similar to that of suspended particles at 20 m; this implies that the larger sinking particles are composed of phytoplankton themselves and receive little alteration during sinking from euphotic to the 140 m layer. The smaller sinking particles show contrasting properties in isotopic values and C/N ratios, compared with the larger ones (Fig. 11). Judging from those signals, the smaller particles are composed of highly degraded organic matter. Though they are trapped in the trap cylinder, they are too small to sink independently; hence it is thought that the smaller sinking particles sink in association with the larger sinking particles. In addition, the suspended particles below the euphotic zone show similar properties with those of smaller sinking particles, indicating that the major source of suspended particles is the smaller sinking particles.

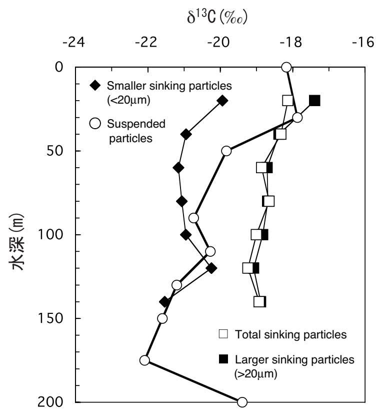

Fig. 11. Vertical profiles for the $\delta^{13}C$ of suspended and sinking particles collected at the upper layer of the Sagami Bay during May 2006.

Laboratory of Bio-Physical Oceanography

Observation of material transport through the eastern channel of the Tsushima/Korea Strait

Enormous fresh water and materials are transported from the East China Sea (ECS) to the Japan Sea (JS). Isobe *et al*. (2002) reported that at least 70% of fresh water in the ECS enters into the JS through the Tsushima Korea Strait (TKS). Therefore, the change of Changjiang river discharge due to the Three Gorges Dam strongly influences the ocean environment not only in the ESC but also in the JS. Although it is certain that the change of river discharge will impact both the ECS and the JS ocean environment, it has not been revealed yet how degree influences the environmental change and how much materials are transported through the TKS. Hence, it is very important for predicting the future environment of the JS to evaluate quantitatively the energy and material transport through the TKS. In the present study, we conducted field observations at two lines where the volume transport of the Tsushima Warm Current can be estimated, and heat, fresh water, chlorophyll, and nutrient transports by the Tsushima Warm Current were evaluated.

Field observations were conducted 15 times at CL and N lines by mainly T/V Tenyo of National Fisheries University as shown in Fig. 1. Since tidal current is dominant in the TKS, average material transports cannot be evaluated by instantaneous current velocity data measured by ADCP. Therefore, it is necessary that tidal signals are removed from ADCP data in order to estimate average material transports. The harmonic constants of tidal currents have been estimated from long-term ship-mounted ADCP measurements at CL line (Takikawa *et al.*, 2003) and from moored ADCP measurements at N line (Teague *et al.*, 2001). It is possible that we can eliminate tidal signals from the instantaneous ADCP data at the two lines and see the vertical structure of the Tsushima Warm Current. At each observation station, we measured water temperature, salinity, chlorophyll a, DO and nutrients by CTD and water sample.

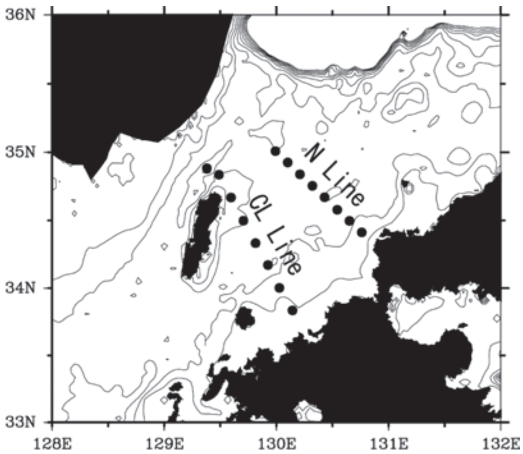

Fig. 1 Observation lines in the TKS.

Material flux and transports through CL and N lines are evaluated from multiplying the current velocity by each component such as water temperature, chlorophyll a, and nutrients. Fresh water flux in the upper layer is large owing to reflecting salinity distribution, and maximum fresh water flux appears as well in the central part of the eastern channel where current velocity is the fastest. As for the nutrient flux, maximum flux appears in the middle layer of the eastern channel because nutrient concentration increases from surface to bottom while current velocity decreases. A cyclonic eddy appears frequently in the eastern channel in summer. Nutrient flux near the cyclonic eddy increases by supplying nutrient from the bottom layer associated with upwelling. Mean volume transport across the CL line from August 2005 to November 2006 is 0.91 (Sv). That value is consistent with the result of Takikawa *et al.* (2005). However, the volume transport on 19 August 2005 is extremely small, 0.16 (Sv), due to counter currents in the surface layer vicinity of Tsushima Island and in the bottom layer vicinity Kyushu. Fresh water transport is highest in summer and then gradually decreases to its lowest in April. Average fresh water transport across the CL line is 21.50×10^6 (kg/s). DIN (Nitrate + Nitrite) transport is larger in summer and autumn and lower in winter and spring. Mean DIN transport across the CL line is 2.76 (kmol/s) and that within the euphotic zone (50 m) is 0.92 (kmol/s). Considering that DIN transport from the Changjiang river is 2.1 (kmol/s) (Zhang 1996), it is suggested that the horizontal transport of DIN by the Tsushima Warm Current plays an important role for the lower trophic ecosystem in the entrance of the JS.

Summertime decrease in water temperature at subsurface layer in Sagami Bay

The frequent occurrence of the summertime decrease in water temperature at the subsurface layer in Sagami Bay is revealed by analysis of monthly CTD data at station S3 (35°00'N, 139°20'E) from January 1997 to July 2004 and historical oceanographic data from 1970 to 2001 (MIRC Ocean Dataset 2005). The intensity and area coverage of the decrease in water temperature change from year to year and vary with depth (Fig. 2a). The depth where this phenomenon occurred is from 20 m to deeper 200 m. Average magnitudes of the decrease in water temperature reach a maximum at depth of around 50 to 100 m and decrease to the surface and deeper layers, while its area coverage is considerably large and may occupy the whole Bay in some cases. The time scale of this phenomenon has not been known yet because all observations are limited to only one or several days a month, but results from CTD and historical oceanographic data reveal that there are some cases with periods longer than one month. This phenomenon plays an important role in the biological processes in Sagami Bay through increasing nutrient and chlorophyll a concentration at the near-surface layer. Although the relationships between the summertime decrease in water temperature and distance to the Kuroshio path from S3 station and between this phenomenon and distance of the Kuroshio path displacement are not highly correlated. However, the Bulletin of Ocean Conditions and other evidence demonstrate that all these events may relate to the appearance and displacement of the cold water mass (or cold eddy) off Enshu-nada under influences of the Kuroshio path variation. This hypothesis is also confirmed by analyzing a numerical model result of Guo *et al*. (2003) (Fig. 2b). The frequent occurrences of cold eddies as well as their displacement along the Japan coast accompanying the Kuroshio path meander are possibly the main reason for the summertime decrease in water temperature at the subsurface layer in Sagami Bay (Fig. 3).

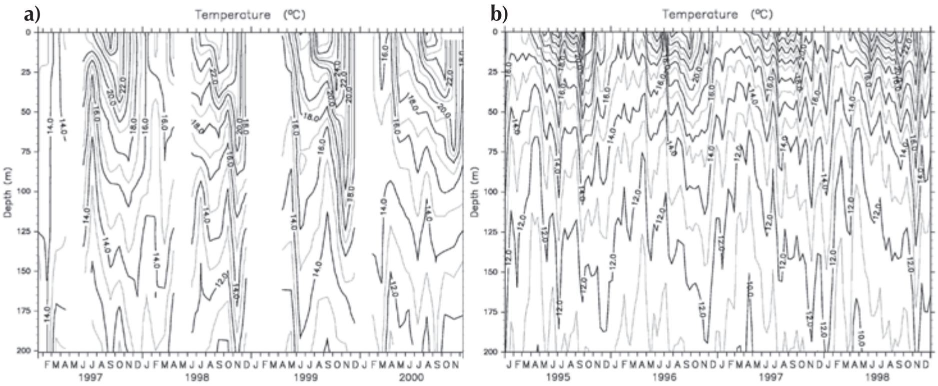

Fig. 2 Time-Depth plot of CTD (a) and Model (b) temperature at station S3 in Sagami Bay.

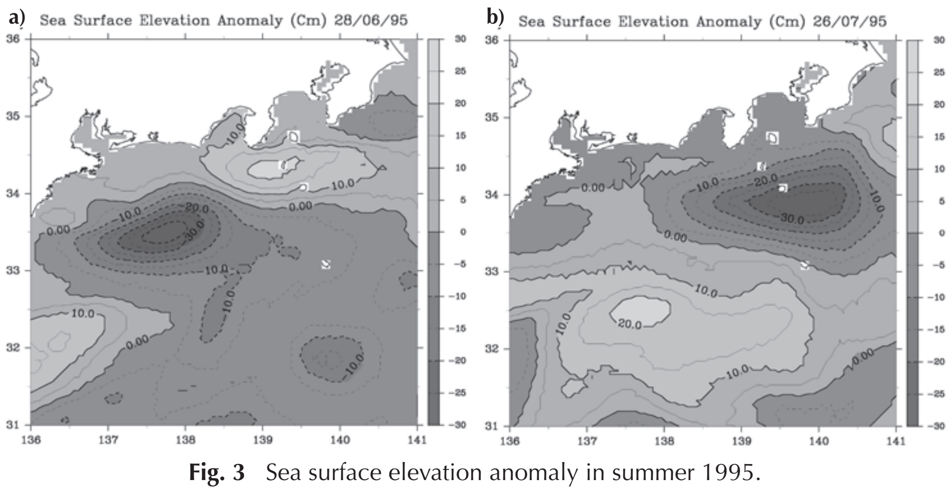

Fig. 3 Sea surface elevation anomaly in summer 1995.

List of Publications

* : Staffs, students and research fellows in the HyARC.

1. Bhatt, B.C.* and K. Nakamura*
A climatological-dynamical analysis associated with precipitation around the southern part of the Himalayas. *Journal of Geophysical Research*, vol.**111**, D02115, doi:10.1029/2005JD006197, 2006.
2. Chiba, S., K. Tadokoro, H. Sugisaki and T. Saino*
Effects of decadal climate change on zooplankton over the last 50 Years in the western subarctic North Pacfic. *Global Change Biology*, Vol.**12**, No.5, 907-920, doi:10.1111/j.1365-2486.2006.01136.x, 2006.
3. Endo, N. and T. Yasunari*
Changes in Low Cloudiness over China between 1971–1996. *Journal of Climate*, **17-9**, 1204-1213, 2006.
4. Endo, N., T. Kadota, J. Matsumoto, B. Ailikun and T. Yasunari*
Climatology and Trends in Summer Precipitation Characteristics in Mongolia for the Period 1960–98. *Journal of Meteorological Society of Japan*, **84-3**, 543-551, 2006.
5. Fujita, K., L.G. Thompson, Y. Kajikawa, Y. Ageta, T. Yasunari*, A. Sakai and N. Takeuchi
Thirty-year history of glacier melting in the Nepal Himalayas. *Journal of Geophysical Research*, Vol.**111**, 2006.
6. Goswami, B.N., G.X. Wu and T. Yasunari*
The Annual Cycle, Intraseasonal Oscillation and Roadblock to Seasonal Predictability of the Asian Summer Monsoon. *Journal of Climate*, **19-20**, 5087-5099, 2006.
7. Ichikawa, H.* and T. Yasunari*
Time-space Characteristics of Diurnal Rainfall over Borneo and Surrounding Oceans as Observed by TRMM-PR. *Journal of Climate*, **19-7**, 1238-1260, 2006.
8. Kummerow, C., W. Berg, J. Thomas-Stahle and H. Masunaga*
Quantifying Global Uncertainties in a Simple Microwave Rainfall Algorithm. *J. Atmos. Oceanic Tech.*, **23**, 23-37, 2006.
9. L'Ecuyer, T.S., H. Masunaga* and C.D. Kummerow
Variability in the Characteristics of Precipitation Systems in the Tropical Pacific. Part II. Implications for Atmospheric Heating. *J. Climate*, **19**, 1388-1406, 2006.
10. Liu, A.Q., G.W.K. Moore, K. Tsuboki* and I.A. Renfrew
The effect of the sea-ice zone on the development of boundary-layer roll clouds during cold air outbreaks. *Boundary-Layer Meteorology*, doi:10.1007/s10546-005-6434-4, 2006.
11. Liu, Y.*, T. Hiyama*, R. Kimura and Y. Yamaguchi
Temporal influences on Landsat-5 Thematic Mapper image in visible band. *International Journal of Remote Sensing*, **27**, 3183-3201, 2006.
12. Liu, Y.*, T. Hiyama* and Y. Yamaguchi
Scaling of land surface temperature using satellite data: A case examination on ASTER and MODIS products over a heterogeneous terrain area. *Remote Sensing of Environment*, **105**, 115-128, 2006.
13. Maesaka, T., G.W.K. Moore, A.Q. Liu and K. Tsuboki*
A simulation of a lake effect snowstorm with a cloud resolving numerical model. *Geophysical Research Letters*, Vol.**33**, L20813, 2006.
14. Masunaga, H.* and C.D. Kummerow
Observations of Tropical Precipitating Clouds Ranging from Shallow to Deep Convective Systems. *Geophys. Res. Lett.*, **33**, L16805, doi:10.1029/2006GL026547, 2006.
15. Masunaga, H.*, T.S. L'Ecuyer and C.D. Kummerow
The Madden-Julian Oscillation Recorded in Early Observations from the Tropical Rainfall Measuring Mission (TRMM). *J. Atmos. Sci.*, **63**, 2777-2794, 2006.
16. Matsui, T., H. Masunaga*, R.A. Pielke Sr., S.M. Kreidenweis, W.-K. Tao, M. Chin and Y.J. Kaufman
Satellite-based Assessment of Marine Low Cloud Variability Associated with Aerosol, Atmospheric Stability, and the Diurnal Cycles. *J. Geophys. Res.*, **111**, D17204, doi:10.1029/2005JD006097, 2006.

17. Moteki, Q., T. Shinoda*, S. Shimizu, S. Maeda*, H. Minda*, K. Tsuboki* and H. Uyeda*
Multiple Frontal Structures in the Baiu Frontal Zone Observed by Aircraft on 27 June 2004. *SOLA* (*Scientific Online Letters on the Atmosphere*), 2006, Vol.**2**, 132-135, doi:10. 2151/sola.2006-034, 2006.
18. Naqvi, S.W.A., H. Naik, A. Pratihary, W.D. Souza, P.V. Narvekar, D.A. Jayakumar, A.H. Devol, T. Yoshinari and T. Saino*
Coastal versus open-ocean denitrification in the Arabian Sea. *Biogeosciences Discussions*, **3**, 665-695, 2006.
19. Sano, T.* and K. Tsuboki*
Structure and Evolution of a Cumulonimbus Cloud Developed over a Mountain Slope with the Arrival of Sea Breeze in Summer. *Journal of the Meteorological Society of Japan*, **84**(4), 613-640, 2006.
20. Saito K., T. Yasunari* and K. Takata
Relative Roles of Large-scale Orograghy and Land surface processes on Global Hydro-climate. Part II. Impacts on Hydro-climate over the Eurasian Continent. *Journal of Hydrometeorology*, **7**, 642-659, 2006.
21. Sakai S., R. Harrison, K. Momose, K. Kuraji, T. Yasunari*, L. Chong and T. Nakashizuka
Irregular Draughts Trigger Mass Flowering in a Seasonal Tropical Forests in Asia. *American Journal of Botany*, **93**(8), 1134-1139, 2006.
22. Sarma, V.V.S.S.*, O. Abe, A. Hinuma* and T. Saino*
Short-term variation of triple oxygen isotopes and gross oxygen production in the Sagami Bay, Central Japan. *Limnology and Oceanography*, **51**(3), 1432-1442, 2006.
23. Sarma, V.V.S.S.*, T. Saino*, K. Sasaoka, Y. Nojiri, T. Ono, M. Ishii, H.Y. Inoue and K. Matsumoto
Basin-scale pCO_2 distribution using satellite sea surface temperature, Chla, and climatological salinity in the North Pacific in spring and summer. *Global Biogeochemical Cycles*, Vol.**20**, GB3005, doi:10.1029/2005GB002594, 2006.
24. Shusse, Y. and K. Tsuboki*
Dimension characteristics and precipitation efficiency of cumulonimbus clouds in the region far south from the Meiyu front over eastern Asian continent. *Monthly Weather Review*, Vol.**134**, 1942-1953, 2006.
25. Sukigara, C. and T. Saino*
A 7-year increasing trend of 15N in sinking particles at the mouth of the Tokyo Bay. *Geophysical Research Letters*, Vol.**33**, No.9, L09607, 2006.
26. Takahashi H.G.* and T. Yasunari*
A Climatological Monsoon Break in Rainfall over Indochina in the Summer and its Influence on the Seasonal March of the Asian Monsoon Circulation. *Journal of Climate*, **19-8**, 1545-1556, 2006.
27. Tao, W.-K., E.A. Smith, R.F. Adler, Z.S. Haddad, A.Y. Hou, T. Iguchi, R. Kakar, T.N. Krishnamurti, C.D. Kummerow, S. Lang, R. Meneghini, K. Nakamura*, T. Nakazawa, K. Okamoto, W.S. Olson, S. Satoh, S. Shige, J. Simpson, Y. Takayabu, G.J. Tripoli and S. Yang
Retrieval of latent heating from TRMM measurements. *Bulletin of American Meteorological Society*, **87**, 1555-1572, 2006.
28. Ushiyama, T., R. Shirooka, T. Chuda, H. Kubota, S. Iwasaki, J. Chen, K. Takeuchi and H. Uyeda*
An isolated cloud band around a typhoon in the western tropical Pacific. *Geophysical Research Letters*, **33**(12), L12808, doi:10.1029/2006GL02100, 2006.
29. Wakazuki, Y., K. Tsuboki* and T. Takeda
Periodic evolution of multiscale precipitation systems developed within a Baiu frontal cloud cluster. *Journal of the Meteorological Society of Japan*, **84**(3), 497-518, 2006.
30. Wang, B., P. Webster, K. Kikuchi, T. Yasunari* and Y. Qi
Boreal summer quasi-monthly oscillation in the global tropics. *Climate Dynamics* (*CD*) **27**, 7/8, 661-675, 2006.

31. Yamada, H. and H. Uyeda*
Transition of the Rainfall Characteristics Related to the Moistening of the Land Surface over the Central Tibetan Plateau during the Summer of 1998. *Monthly Weather Review*, **134**(11), 3230-3247, 2006.
32. Yasunari, T.*, K. Saito and K. Takada
Relative Roles of Large-scale Orograghy Land surface processes on Global Hydro-climate. Part I. Revisit to Role of Land-Atmosphere Interaction on Asian Monsoon System. *Journal of Hydrometeorology*, **7**, 626-641, 2006.
33. Yasunari, T.* and T. Miwa
Convective Cloud Systems Over the Tibetan Plateau and their Impact on Meso-scale Disturbances in the Meiyu/Baiu Frontal Zone — A Case Study in 1998 —. *Journal of the Meteorological Society of Japan*, **84-4**, 783-803, 2006.
34. Zhang, C.Z.*, H. Uyeda*, H. Yamada and B. Geng
Characteristics of Convections of Medium Depth to South of the Meiyu Front Analyzed by Using Numerical Simulation. *SOLA* (*Scientific Online Letters on the Atmosphere*), Vol.**2**, 160-163, doi:10.2151/sola.2006-041, 2006.
35. Zhang, C.Z.*, H. Uyeda*, H. Yamada, B. Geng and Y. Ni
Characteristics of Mesoscale Convective Systems over the East Part of Continental China during the Meiyu from 2001 to 2003. *Journal of the Meteorological Society of Japan*, **84**(4), 763-782, 2006.

Hydrospheric Atmospheric Research Center (HyARC)
Nagoya University

Furo-cho, Chikusa-ku, Nagoya 464-8601, Japan

Office:

Telephone: +81-52-789-3466

Facsimile: +81-52-789-3436

Home Page: http://www.hyarc.nagoya-u.ac.jp/hyarc/

The 2006 Annual Report was published December 2007 by the Hydrospheric Atmospheric Research Center (HyARC) Nagoya University. Copies of this report are available from the office of the Center.

Printed by Nagoya University COOP

HyARC

Hydrospheric Atmospheric Research Center, Nagoya University